Synthesis and Characterisation of Au/Fe_2O_3 Catalysts

Ian P. Silverwood

A thesis submitted for the degree of Master of Science

University of Edinburgh 2002

Abstract

Iron oxide supported gold catalysts, and control samples containing no gold, were prepared by the “as-precipitated” method and by the “solution combustion” method. These were studied using BET isotherm, powder and single crystal XRD, TEM, SEM, EDS, XPS and *in situ* DRIFTS. Measurements of activity for the oxidation of CO were carried out using a tube reactor attached to a residual gas analyser.

BET surface areas varied from 37 to 134 m^2/g, with XRD patterns showing the production of haematite, and γ-Fe_2O_3 or magnetite. Scherrer analysis of the gold peaks gave gold crystallite sizes between 42 and 139nm. Assessing the size of gold particles by TEM gave values between 14.0 and 29.7nm. SEM of the samples indicated some very large gold particles on some catalysts and that all samples had a similar physical support structure.

The catalysts produced were of variable activity for CO oxidation, although none were as active as certain nominally similar materials previously reported in the literature.

The more reactive samples had the higher surface areas and XPS showed that the more active catalysts contained gold in the cationic state, with DRIFTS showing the presence of a broad band at $2005cm^{-1}$ due to adsorbed CO on the more active catalysts.

Declaration

I certify that this thesis has been composed by me, and unless otherwise stated, the work presented was performed by me in the Chemistry Department of the University of Edinburgh.

Ian P. Silverwood

Acknowledgements

Primarily I would like to thank Dr Gordon McDougall, who gave me the chance to undertake this degree, kept my enthusiasm up, and was patient when the results were rubbish. After all this, he still wants to keep me on for another three years or so, and for that I am very grateful.

Thanks also must go to Dr Ron Brown, for knowing everything about every piece of scientific apparatus ever made, including how to make dead equipment come to life, and for showing me a little of what he knows.

A very big thank-you to Alex Cook, in whose footsteps I follow, and who has been a father figure to me over the past year. Thankfully I couldn't cause him to tear his hair out, as it departed of natural causes many years ago. If it hadn't then, it would now. Cheers for the patience.

Further, I must thank the microscopists that helped me to obtain passable pictures of my samples. Thanks to John Findlay, Nicola Cayzer and Dr Paula McDade.

Next, a shout out to the rest of the people in the office that made the last year fun. Cheers to the newly crowned Dr Trish Richardson, Neil "tell me a story" Speirs, Madeline Chapman, Dr Li Juan song and Dr Georges Onyestyak Also thank-you to the hangers-on from elsewhere in the department; Alice, Katrina, Dave, Gordon and Hilary.

Finally, thanks to the non-scientists that provided perspective and kept me sane, namely my family and Tabitha. This is for you.

Courses and Conferences Attended

Physical Chemistry Colloquia

Catalytic Club	Firbush Point field centre	May 2001
Physical Section Meeting	Firbush Point field centre	June 2001
Surcat Ecosse	St Andrews	July 2001
Retirement Meeting for Prof. C. Rochester	Dundee	September 2001

Contents

List of figures

Chapter 1

Chapter 2

Chapter 3

Chapter 4

List of tables

Chapter 2

Chapter 3

Chapter 4

Chapter 1: Introduction

1.1 Use of gold for carbon monoxide oxidation

Traditionally gold has been considered as mostly inert, hence its title as a noble metal. In 1952 Trapnell reported it to be the only metal not to adsorb oxygen or hydrogen [1] although this was later disputed [2]. There was then only limited interest in the action of gold as a catalyst, although experiments were carried out using gold for reactions such as the oxidation of NO with CO [3] and alkene oxidation [4]. These experiments had mixed success and limited application. In 1977 however, Ozin *et al.* studied the interaction of single gold atoms with CO at very low temperatures in matrix isolation experiments and showed that the metal could be highly active for the oxidation to carbon dioxide at low temperature [5]. This stimulated interest into the use of finely divided gold as a catalyst for this reaction, and in 1987, Haruta *et al.* synthesised the first highly active gold catalyst for carbon monoxide oxidation [6].

The removal of carbon monoxide by oxidation is of great importance in a number of applications due to the high toxicity of the gas. Carbon monoxide is formed when carbon containing compounds are oxidised in an environment with a low concentration of oxygen. This may be due to fuels burnt with poor ventilation or natural processes such as forest fires or volcanic eruptions. Emissions of CO due to incomplete combustion have to be minimised, whether from vehicle exhausts, gas fires or industrial sources. The oxidation of CO is also important in purifying other gas streams. In a fuel cell, CO can poison the anode for oxidation of hydrogen, and a highly selective catalyst is therefore needed. Gold on α-Fe_2O_3 has been investigated for this by Schubert *et al.* to remove the CO whilst not oxidising H_2 [7]. The reduction of nitrogen oxides has also been studied [8].

This flexibility of application for the gold catalysts, and the possibility of tailoring their selectivity makes them very attractive industrially. Add to this the more exotic uses, such as in sealed CO_2 lasers, [9] and removal of odours in Japanese toilets [10,11] and it is no surprise that further investigation is ongoing.

1.2 Syntheses of gold catalysts

The first reported practical catalysts were created by Haruta [6] in 1987, by the coprecipitation method, using iron, cobalt and nickel oxides precipitated with Na_2CO_3. By 1996, a number of other methods had been demonstrated to produce active catalysts, and these are summarised below.

1. Coprecipitation [6]

An aqueous solution of $HAuCl_4$ and a metal nitrate is poured into an aqueous solution of Na_2CO_3 (or NH_4OH). This yields a carbonate or hydroxide precipitate, which is washed, dried and calcined in air to obtain gold supported on a metal oxide.

2. Deposition precipitation [12]

The pH of a solution of $HAuCl_4$ in water is adjusted to a point between 6 and 10. A metal oxide support is then immersed in the solution and aged for a number of hours. The support may be in a number of forms, such as powder, bead, thin film or monolith. If the temperature and concentrations are properly chosen then $Au(OH)_3$ is deposited exclusively on the support phase. The precursor is then treated as in coprecipitation, in that it is washed, dried and calcined.

3. Chemical Vapour Deposition (CVD) [13]

A metal oxide support is heated in vacuum and a gaseous organic gold precursor, typically dimethyl-gold(III)-acetyl acetonate, is introduced. This undergoes decomposition on contact with the support to leave gold particles. This method allows synthesis over a wider range of metal oxides, whereas the liquid phase preparations tend to fail on acidic metal oxides such as SiO_2.

4. Co-sputtering [14]

In an oxygen containing atmosphere, gold and metal oxide are simultaneously sputter-deposited onto a substrate, leading to the formation of a thin film. The film is then annealed in air.

5. Impregnation [15]

A support is immersed in a solution of $HAuCl_4$ for a number of hours with stirring, then removed and dried. Although this usually resulted in poorly active catalysts, in 1995, Bollinger and Vannice [15] claimed to have found activity using a titania supported catalyst when a three stage pre-treatment was used. They found that the sample was active if reduced at high temperature, calcined, and then reduced again at low temperature.

6. Impregnation on as-precipitated supports[16]

In 1996 Iwasawa *et al* demonstrated a new method for the production of very active catalysts by impregnating a separately precipitated wet metal hydroxide support with an organometallic gold precursor [16]. Co^{2+}, Fe^{3+}, Ni^{2+}, Zn^{2+} Mg^{2+} and Cu^{2+} hydroxides were hydrolysed from an aqueous solution of the metal nitrates with a sodium carbonate solution. Titanium hydroxide and vanadium hydroxide were similarly prepared from titanium-tetra-*iso*-propoxide and vanadium trichloride. Phosphine stabilised gold was introduced as $AuPPh_3NO_3$ [17] or $Au_9(PPh_3)_8(NO_3)_3$ [18] The $AuPPh_3NO_3$ was dissolved in acetone and the $Au_9(PPh_3)_8(NO_3)_3$ in methanol, then impregnated onto the hydroxide supports with vigorous stirring. They were dried under vacuum, then calcined at 673K under a flow of air. At this stage the nitrate dissociates, and leaves gold phosphine cations [19]. The OH groups on the metal hydroxides bond to the phosphine groups, [20] and this interaction before calcination was suggested to be very important for the creation of highly active catalysts [21]. It is proposed that the high affinity of the ligand for gold prevents agglomeration and sintering, as it inhibits interaction between the gold atoms [22].

However, the presence of triphenylphosphine in the calcination step has also been shown to affect the morphology of the support [19]. This is also proposed as a factor, as the catalysts are far more effective when the support is amorphous [21]. Calcination decomposes the hydroxides to the oxides and the phosphine complexes are oxidised and lost. When the organic complex is supported on the wet hydroxide, it is more stable thermally than on Fe_2O_3 [20]. This effect causes the transformation of the support and the loss of the metal ligand to occur at similar temperatures, (473-573K) and it therefore follows that there is greater influence of the organic compound over the support

Haruta reported that methods one to four produced hemispherical gold particles that are strongly attached to the oxide support by their flat planes, and claimed this was the reason for their high activity [23]. A typical TEM is shown below in Fig. 1.1. It was also proposed that this demonstrated the gold was more thermally stable than supported gold without this interaction, with the reason for this morphology being the stronger affinity of the precursors to the support. However, it was noted that some samples were not as active as others and this was ascribed to contamination by Na^+ [24] and Cl^-, [25] which will be discussed later, in section 1.4.1

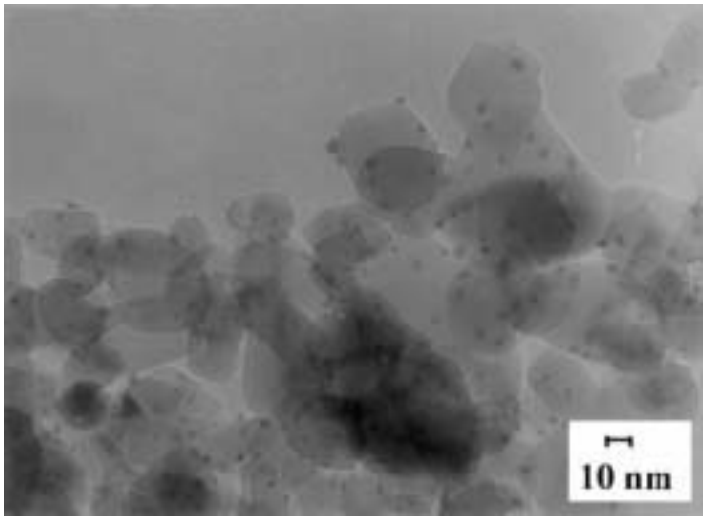

Fig. 1.1: Transmission electron micrograph of Au/TiO2 catalyst by Haruta prepared by deposition-precipitation [12]

The need for a calcination step in the synthesis of supported gold catalysts is an issue that most groups involved in the synthesis of active gold catalysts are agreed on. Haruta originally calcined the first catalysts at 673K [6], and later claimed that calcination at temperatures above 473K was needed to remove Cl^-, which poisoned the catalyst. The most commonly adopted temperature for calcinations is 673K, although some workers in this area disagree that Cl^- is a poison [26] and a few believe that calcination at high temperature actually decreases activity [27]. These workers have found that the active gold species is oxidic gold, which is converted to metallic gold by calcination.

1.3 Supports

A wide range of metal oxides as supports have been studied for the oxidation of CO over supported gold catalysts. By varying the support for the gold, a high range of control over the reactions is available, although the reasons for this are unclear. Recently Schubert and co-workers undertook research into the necessary requirements for the support, concluding that they could be split into two groups, the active, and the inert [28]. Active support materials are Fe_2O_3, TiO_2, NiO_x and CoO_x. These are, therefore, the subjects of most research, although alumina, [26] silica, [29] ceria, [30] zeolites, [31] MgO [29] and ZnO [30] have also been investigated. Of all the supports, Fe_2O_3 is particularly interesting, as the support in an Au/Fe_2O_3 catalyst can adsorb a large quantity of oxygen, suggesting this is how it is supplied to the reaction [28]. Schubert succeeded in demonstrating the difference in support efficiency by creating a number of catalysts with mixed supports containing “active” (Fe_2O_3) and “inert” (MgO) in varying proportions. They found that for the Fe_2O_3-containing catalysts the activity varied with the proportion of Fe_2O_3 present. For the catalysts on “inert” supports, the activity was dependent on the gold particle size [28]. Another interesting property of supported gold catalysts is the ability to “tune” them for preferential or non-preferential oxidation by selection of the support.

Alumina support has low activity, but is not selective between H_2 and CO, whereas iron oxide support leads to a catalyst that is relatively much higher in activity for CO oxidation [32].

However, due to the precipitation step, consistent synthesis of supports between groups is difficult, especially in the case of iron, as there are 16 different iron oxides, hydroxides and oxide hydroxides. Hydrolysis is not the most reliable method of production, as addition of base leads to local pH gradients, to which the synthesis is very sensitive [34].

It is reported that not only are supported iron oxide catalysts selective for CO oxidation, but that they are also incredibly active. The reports of Iwasawas group of as-precipitated iron oxide catalysts being amongst the most active prompted further study, [16] particularly as their results were not duplicated elsewhere in the literature. Thus Iwasawa's method was adopted for the production of most of the catalysts and the study of gold supported on iron oxide was chosen. Further synthesis using the solution combustion method was investigated, due to the novelty of the method and the successful production of various supported metal oxide catalysts in this manner [36,38,40].

1.4 Morphology of Au/Fe_2O_3 catalysts

1.4.1 State of support

From his initial involvement in the synthesis of highly active supported gold catalysts in 1996, [60] Iwasawa continued investigation of as-precipitated catalysts and later undertook a thorough review, relating studies in SEM, TEM, TGA, XRD, FT-IR, EXAFS, XPS and Raman spectroscopy to catalytic activity [19]. It is claimed within the paper that only α-Fe_2O_3 is formed by the co-precipitation method. With the presence of the triphenylphosphine ligand in the gold complex both α and β phases of mixed valence Fe_3O_4 are formed.

This leads to formation of amorphous Fe_2O_3 when calcined, with both α-Fe_2O_3 and γ- Fe_2O_3 detected. The paper further states that an amorphous support is beneficial for high catalyst activity, suggesting that the organometallic precursor causes this by bonding to defects and hydroxyls in the crystal lattice.

It has been suggested that impurities influence the nature of the support and increase activity of the final catalysts by providing more defect sites [21]. The role of impurities in the support is, however, controversial. Haruta claims that Cl^- and Na^+ act as poisons to gold catalysts whereas Bethke and Kung [26] claim no effect for Cl^-, Pt, Ir and Mg contained in deposition-precipitated Al_2O_3/Au catalysts. In even starker contrast, Iwasawa *et al.* [30] claim that Na^+ acts as a promoter, and Gupta *et al.* [33] report that a synthesised chloride free catalyst was less active than the corresponding chloride containing sample.

The drying and calcination of the support after precipitation involves a number of recrystallisation steps [19]. Mixed valence Fe_3O_4 is first created upon drying, with formation of γ- Fe_2O_3 at temperatures greater than 473K and α-Fe_2O_3 at greater than 673K. It is suggested that the change in support morphology allows the metal-support interaction to be formed.

1.4.2 State of Gold

It is generally agreed through TEM photographs that gold is actively dispersed as near hemispherical particles attached to the support on its flat face [35,12]. Baiker *et al.* [37] suggest that the shape is a sphere, flattened on one side, with the contact angle dependant on the support. It is taken that the interaction with the support is therefore strong, both physically and electronically, which then has important implications for the mechanism. An area in which there is less agreement is the oxidation state of the active gold. Iwasawa's as-precipitated samples have active gold in the metallic form, [20] but Park and Lee claim oxidic gold as the active species on deposition-precipitated Fe_2O_3, TiO_2 and Al_2O_3 [39].

Visco *et al.* [41] claim that both forms of the gold on Fe_2O_3 are active, finding that co-precipitation gives both forms, whereas deposition precipitation leads solely to metallic gold.

1.4.3 Relating form to function

To summarise what is thought; the gold is supported as very fine particles, probably as hemispheres and in good contact with the support, both electronically and physically. A number of explanations have been proposed for why the gold will catalyse the reaction in this form but not in the bulk, each relying on aspects of the above description. It is agreed that small gold particles are associated with higher activity, and each theory is compatible with this.

The first theory, proposed by Haruta, [23] is that of a boundary mechanism. This theory was further developed and characterised by Frost by studying the Schottky junction effect on thoria supported copper [42]. By bonding with a metal oxide support, the electronic properties of the gold are changed at the boundary with the support phase. A familiar example of this effect is the so-called depletion zone in semiconductor diodes. Where two substances of different electronic potentials meet, the electrons will seek to find the lowest energy state, and thus will transfer from one material to the other. This charge transfer results in a zone at the junction where the energy of the electrons varies with the distance from the junction, as can be seen in Fig. 1.2. This alteration of the electronic structure encourages the catalytic reaction to occur. In the case of gold/metal oxide catalysts the catalytic activity is thought to arise from modification of the electronic structure of the metal compared to that of the bulk gold at the junction between the metal particle and the support oxide. The gold acts as the p-type material, and the support as the n-type. As the particle size decreases, more boundary is produced, and less bulk phase gold is present, thus explaining the increase of reactivity with decrease in particle size.

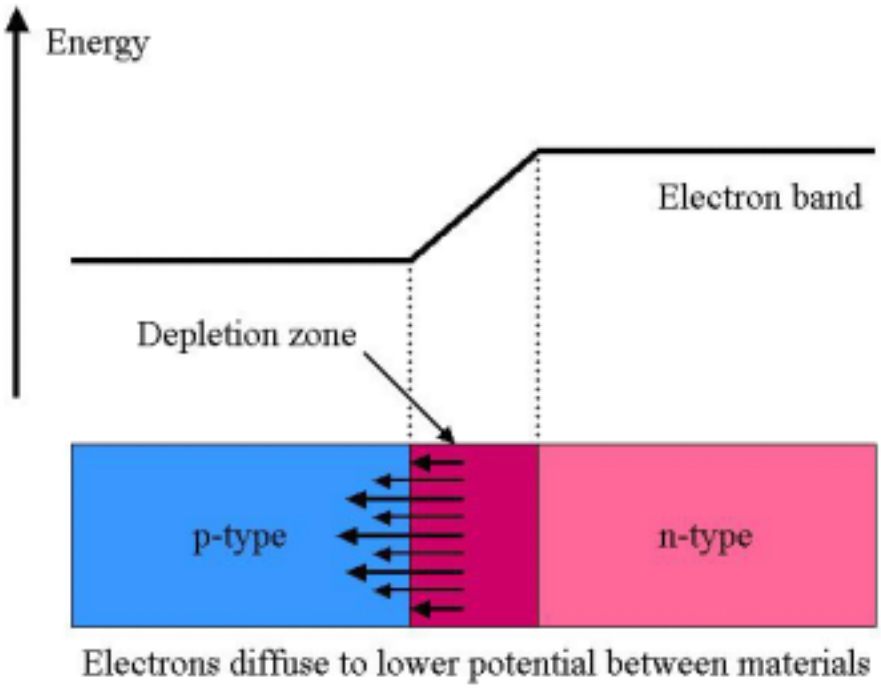

Fig. 1.2 Representation of the Schottky junction

The second theory is based on a size effect. Reactions occur faster when there is a high surface area due to the fact that a surface is a high-energy state for the atoms. As the particles become smaller, this is a greater effect as the atoms are forced into energetically unfavoured sites, such as edges, steps and corners, that are increasingly less characteristic of the bulk metal. This effect has been demonstrated in that oxygen, which will not normally chemisorb on gold, does so if the particles are small enough [43]. A third explanation, which also relates activity to catalyst metal particle size is a quantum size effect, shown to occur by Valden, [44] and is based on band theory. Normally the electronic structure of metals is taken to be a series of broad bands caused by the overlap of a great number of single atomic orbitals. However, as the metal particles become smaller and smaller, the number of atoms and hence orbitals becomes smaller. At some point, we can no longer think of these orbitals as a continuous band. Below a certain number of atoms in a cluster, or a size of particle we can no longer use band theory. At this point, due to a quantum size effect, the metal essentially becomes a non-metal. It is this change in electronic structure that allows the catalyst to function.

A final theory, put forward by Gupta *et al.* suggests that the gold is not active at all [33]. Instead they propose that the chemisorption of CO on the gold particles is sufficiently exothermic to heat the surrounding support to a high enough temperature for the reaction to occur there. This localised heating effect would not result in significantly higher average temperatures, but would boost the free energy near the gold particles high enough to cause reaction on the iron oxide. The smaller the gold particles, the more efficiently heat is transferred to the support.

1.5 Mechanism

The above section summarises the potential theories as to why the catalyst works, but do not throw any light on the mechanism of the reaction. A number of mechanisms have been proposed for the reaction, although the area is still under discussion. These are summarised in Fig. 1.3.

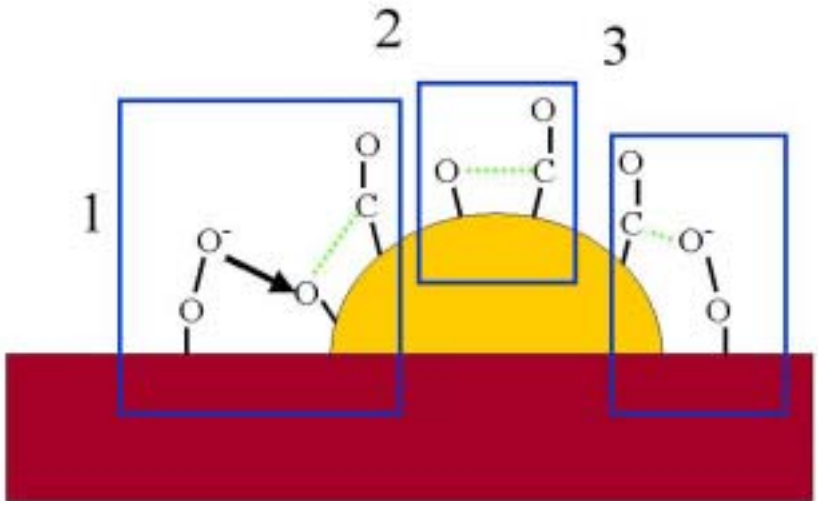

Fig. 1.3: Proposed reaction mechanisms of supported gold catalysts

Most mechanisms agree that the important aspect of the catalysts is the interface, as bulk gold is unreactive. Haruta suggested that the activity of the catalyst depended on the length of the interface perimeter, as the turnover frequencies for the catalysts increased with the inverse of the square of gold particle diameter ($1/D_{Au}$) [35].

With this evidence he suggested a mechanism where CO adsorbs on gold, and molecular oxygen adsorbs on the support [23]. Haruta also interprets data from IR spectra to show carbonate intermediates in the reaction [35].

This explains the importance of the perimeter, but it is not made clear whether the reaction occurs with spillover oxygen on gold, (1 in Fig. 1.3) or with the oxygen adsorbed on the support. (3 in Fig. 1.3) Using radioactively labelled oxygen Boccuzzi *et al.* found evidence for the reaction of CO and oxygen reacting when adsorbed on the same gold site [45] on ZnO supported catalysts, although this has been contradicted by Schubert and co-workers, who suggested that the method used was flawed [28]. Instead, they propose two mechanisms. For the inert supports, they suggest that reaction occurs between both species adsorbed on gold, (route 2 in Fig. 1.3) using the evidence that the reactivity is highly sensitive to gold particle size and the dissociation of oxygen on gold has a high energy barrier. For the active supports they propose that the reaction occurs with support oxygen, (route 3 in Fig. 1.3) having found evidence that highly mobile molecular oxygen adsorbs on the support, probably as the superoxide species. This theory is in agreement with the findings of Iwasawa's group [46,47,48] and Claus *et al.* found that the activity of gold supported on titania and zirconia was dependant on the concentration of F-centres (electrons trapped in oxygen vacancies in the support lattice). These sites are highly attractive for oxygen bonding, and are formed around the gold particles due to the Schottky junction [42].

Chapter 2: Experimental

2.1 Synthesis

Four Au/Fe_2O_3 catalysts were prepared, three of which generally followed the method of Iwasawa *et al* [21]. Briefly, triphenylphosphine gold nitrate was synthesised from triphenylphosphine gold chloride and silver nitrate, then dissolved in acetone and impregnated on iron oxide that was still wet prepared by hydrolysis of iron trinitrate. The specific details of the synthesis are set out below

Two batches of the catalyst were prepared according to the as-precipitated method as below (as-precipitated method 1), and denoted Cat1 and Cat2. 0.33g (0.66 mmol) of $AuCl(PPh_3)$ was dissolved in 7ml dichloromethane (DCM) and added dropwise to stirred solution of 0.228g $AgNO_3$ (1.34 mmol) in 21ml methanol to form $AuPPhNO_3$ This was stirred for three hours, then filtered through a fritted filter with 1cm layer of celite to remove AgCl, then washed through with 10ml DCM. The combined solution was evaporated to dryness on a rotary evaporator, then 15ml DCM was added, and the solution filtered as before. This was again evaporated to dryness, this time on a vacuum line. The solid residue was dissolved in a minimum of DCM, and then three times this amount of absolute ethanol was added. This was stirred under a slow stream of nitrogen until white crystals formed. These were filtered and washed, (3x5ml absolute ethanol, 3x5ml diethyl ether) before being dried under vacuum. When poor yield were obtained, the mother liquor was recovered, and stored in a freezer. Crystals grown from this were recovered and washed in the same way. A total typical yield after all crops was 25%.

$Fe(OH)_3$ was then synthesised according to the yield of $AuPPhNO_3$ crystals to give a 3% loading of gold by weight. $Fe(NO_3)_3.9H_2O$ (*circa.* 4g) was added to Na_2CO_3 solution (1.5g in 30ml H_2O) The resulting precipitate was washed with de-ionised water until the pH was neutral, then filtered, but not allowed to dry.

The $(PPh_3)AuNO_3$ crystals synthesised were dissolved in acetone and added to the wet $Fe(OH)_3$, then vigorously stirred for twelve hours to impregnate the support. This was then held under vacuum for 5 hours to remove solvent. The resulting powder was heated to 673K at a rate of 4K/min, then held at 673K for four hours under a flow of air (rate = 30 ml/min). A blank iron oxide sample (denoted Blank1) was also prepared by hydrolysis of iron nitrate. The wet precipitate was stirred in acetone, then calcined, although no source of the gold $AuPPh_3(NO)_3$ complex was present in the synthesis.

Gold loadings were estimated assuming that all of the gold had been incorporated in to the catalysts, giving loadings of 2.94 and 3.73% by weight for Cat1 and Cat2 respectively.

The above synthesis was adapted following correspondence with Iwaswa [49] to mimic the successful synthesis as closely as possible. Photodecomposition of the precursors was minimised by covering all of the vessels used in aluminium foil. Premature decomposition of the gold precursors was further discouraged by minimising exposure to heat. The $AuPPhNO_3$ was stored in a freezer, until required and evaporation on a Schlenk line was used instead of rotary evaporation.

The synthesis of the support was also carried out more rigorously. 7.399g Na_2CO_3 was dissolved in 200ml water, and stirred vigorously. A solution of 8.399g $Fe(NO3)_3.9H_2O$ in 400ml water was added dropwise to this and aged with stirring for three hours. This was filtered and washed until the washings were neutral. The iron hydroxide was left on the filter until the surface started to crack. The wet $Fe(OH)_3$ was then taken and ground in 100ml acetone, then stirred in foil covered flask for 30mins-1hr. The acetone solution of the gold complex was added, then the acetone evaporated under vacuum for about 4 hrs to ensure dryness.
This mixture was calcined as before, but the air was passed through a 60cm stainless steel tube filled with MS-5A that had previously been dried with nitrogen at 653K for two hours. This sample was denoted Cat4 and the synthesis as-precipitated method 2. Gold loading was estimated as before, giving 6.37% by weight.

The second synthesis for the catalyst was radically different and inspired by work by Patil *et al*. [50]. The combustion synthesis method has been used to create catalysts with metal nanoparticles such as Pt, Pd, Ag, Au and Cu supported on Al_2O_3 and CeO_2. These have been demonstrated to catalyse the reactions of NO reduction and the oxidation of CO and hydrocarbons [36,38,40,51]. It was hoped that applying this method to the production of Au/Fe_2O_3 would result in a much faster route to the highly active gold catalysts. In this method the reactants were dissolved in a minimum of water, with heating and stirring, and placed in muffle furnace maintained at 350^oC. This caused the water to evaporate and the mixture left to combust and give the product. 7.6g $Fe(NO_3)_3$ and 3.5g $C_2H_6N_4O_2$ were used to create a blank iron oxide (Blank5). 7.6g $Fe(NO_3)_3$, 3.5g $C_2H_6N_4O_2$ and 0.05g $HAuCl_4$ were used to synthesise a gold containing catalyst that was denoted Cat3, with an estimated gold loading of 1.52% by weight. The sources and purities of the chemicals used in all syntheses are presented in Table 2.1.

Compound	Supplier	Purity
$AuPPh_3Cl$	Strem	98%
$AgNO_3$	Acros	99.8%
$Fe(NO_3)_3$	Riedel de Haen	98%
$NaCO_3$	Fisher	99.5%
$HAuCl_4$	Acros	98%
Oxalyldihydrazide	Acros	98%

Table 2.1: Purity and source of chemicals for synthesis

2.2 Characterisation

2.2.1 Surface area

Gas molecules can attach, or adsorb, to a solid surface in two ways, physically and chemically. These are normally abbreviated to physisorption and chemisorption. Physisorption is simply a weak van der Waals interaction, whereas chemisorption involves chemical bonding. This change in the bonding orbitals of the gas is one reason why catalysis occurs at surfaces. A number of models, or isotherms are available to describe the adsorption of gases to solids, and relate the fractional coverage (θ) to the gas pressure. For catalysis, the higher the surface area, the better, as the more surface is in contact with the reactant, the greater the effect of the catalyst will be. Surface area measurements were carried out in a similar manner to the literature, [21] to allow easy comparison with results from other groups and catalysts. The sample was pre-treated at 368 K for one hour and 573K for three hours under nitrogen, and then a conventional 5-point BET nitrogen isotherm was taken at 77K. All measurements were carried out on a Micromeretics Gemini analyser. The analyser has two identical tubes maintained at the same temperature in the same dewar of liquid nitrogen. The analysis gas (nitrogen) is admitted to the sample tube *via* a servo valve. Delivery of gas to the balance tube is controlled by another servo valve coupled to a differential pressure transducer. This measures the pressure imbalance between the two tubes due to the adsorption of nitrogen onto the sample. As the sample adsorbs gas, pressure in the sample tube drops, and the servo admits more nitrogen to restore the pressure to equal that in the balance tube. This ensures that gas is admitted to the sample only as fast as the gas is adsorbed, and thus the sample is under a constant gas pressure. The amount of nitrogen admitted to the sample is logged and the surface area calculations are carried out by the analyser.

2.2.2 X-Ray Diffraction

2.2.2.1 Powder XRD

X-rays are a form of electromagnetic radiation with a wavelength of the order of 10^{-10}m (1Å). This allows the waves to be diffracted by an aperture of the same size. Fortunately the distance between atoms in a crystal is of this magnitude and so X-rays can be diffracted by crystals. In powder XRD the angle of the sample to incident radiation is varied in one dimension and the intensity of the reflected beam is measured. The maxima of the pattern are related to the distance between the crystal planes in accordance with Braggs law; $n\lambda=2d \sin \theta$, where n is an integer and d is the crystal plane separation, often simply called the d-spacing. The d-spacings give a characteristic pattern of lines that can be compared with data in standard files [52] and used to identify compounds and their morphology. X-ray diffraction works best for compounds that have well defined crystal planes and long-range order. Small particles and amorphous samples lead to broad peaks and low intensity. However, this can be used in a positive way. By measuring the degree of broadening of the peaks, an estimate of the mean crystallite size is can be calculated. This may be different to the particle size, as there can be different crystalline regions in one particle. This effect is governed by the Scherrer equation, named after one of the pioneers of X-ray diffraction:

$$L = \frac{K\lambda}{\beta \cos\theta}$$

L represents the mean crystallite size, β is the peak broadening at half height and K is a constant, close to one, dependant on the shape of the particles. For spheres it has the value 0.893. However, this does not take into account the fact that the instrument will cause some sort of line broadening, as an infinitely thin line is an impossibility. To counteract this fact, a sample of a highly ordered material is used, such that the effect of line broadening due to crystal size can be ignored.

This will give the instrumental line broadening, which is then simply subtracted from the peak width measured to give the braodening due to the particle size. The empty aluminium sample holder was used for this purpose. A Phillips powder diffractometer PW1730 (40kV, 30mA), using the copper K_α line at 1.5418Å, was used in all of the studies detailed.

2.2.2.2 Single Crystal X-Ray Diffraction

X-ray crystallography varies from powder XRD in that a single crystal of the sample is used and therefore normally only pure crystalline materials can be studied. A suitable crystal is mounted on a goniometer that varies the orientation of the crystal to the incident angle of the X-rays. Unlike powder XRD this is varied in three dimensions so that more information can be obtained. It is possible by this method to obtain the exact positions of each atom in the crystal, so that not only the spacings between planes are obtained, but also the complete crystal structure, including the unit cell.

2.2.3 Electron microscopy

2.2.3.1 Transmission Electron Microscopy (TEM)

The instrument used for TEM was a Phillips CM120 Biotwin 120KV, capable of resolution greater than 0.34nm and magnification of 2 million. Samples were prepared by grinding the sample in an agate pestle and mortar, then suspending them in ethanol. A drop of the suspension was then placed on a Formvar carbon coated 300-mesh grid and introduced to the microscope. Gold particles turn up as intense dark spots on the TEM negatives, and allow us to size the supported gold particles, as well as their distribution.

2.2.3.2 Scanning Electron Microscopy (SEM)

SEM has a great depth of field that allows an easily interpreted three-dimensional view. Different detectors in the SEM allow different views. For viewing morphology the secondary electron detector was used. Secondary electrons are emitted when the electron enters the surface of the sample, and causes other electrons to be ejected. These depend on the topography of the surface and a three dimensional view can be generated. The back-scattered electron detector detects electrons that are instead scattered back towards the incident electron beam. As the amount of backscatter depends on atomic mass, this shows gold in high contrast to the support. The SEM used was a Philips XL30CP fitted with an Oxford Instruments Isis 300 X-ray analyser, allowing Energy Dispersive X-ray Scattering (EDXS) analysis.

When a sample is bombarded by electrons in the SEM, X-rays are emitted. These X-rays are specific to each element, allowing identification of the elements in the sample. The intensity of X-ray emission is not uniform, so only a semi-quantitative interpretation can be used. Lighter elements are harder to resolve, as the x-ray peaks produced are of similar low energies. Thus the system only allows identification of atoms heavier than nitrogen. Samples for the SEM were attached to aluminium stubs using adhesive carbon discs from Agar Scientific.

2.2.4 X-ray photoelectron spectroscopy (XPS)

The technique of XPS depends on a phenomenon called the photoelectric effect. If light of a sufficiently high frequency is used to illuminate a sample, electrons will be ejected. The energy of the light needs to be greater than the sum of the binding energy of the electrons and the work function. The work function is the energy needed to remove an electron from the sample to vacuum, or more rigorously the difference in energy between the Fermi level of the material and the energy of the electrons in vacuum.

The instrument measures the kinetic energy of the ejected electron, which is equal to the energy of the incident light, less the binding energy of the electron and the work function. If the work function is known, the binding energy can be easily calculated. As the work function varies with the sample charge, which can change as the electrons are ejected, the spectra are referenced against a peak of known energy, normally the peak due to carbon at 284.6 eV. The energy of the illumination for photoelectron spectroscopy is chosen to select the orbitals of interest. Ultraviolet light of lower energy is used to view more weakly bound valence electrons and the technique then is UPS (Ultraviolet Photoelectron Spectroscopy). XPS uses shorter wavelength X-rays and ejects both valence electrons and the more tightly bound core electrons. This allows for identification of elements and oxidation state. XPS is a surface sensitive technique, not due to the depth the x-rays can penetrate, but the distance a free electron can travel in the solid. The inelastic mean free path (IMFP) of an electron in a solid is a function of the kinetic energy of the electron. For the range of kinetic energy of electrons generated in the XPS experiment the IMFP is of the order of 50 angstroms. Statistically 90% of the emitted electrons will come from with 2 IMFP, giving 100 angstroms as the maximum 'sampling depth'.

The samples were run using a Thermo VG Scientific Sigma Probe with a 1486.6eV Al K_α plate source and a flood gun for charge neutralisation. The materials were mounted on adhesive carbon pads (Spectro Tabs obtained from Agar Scientific) on modified SEM stubs. Background spectra were obtained from an empty section of the pad.

2.2.5 Infra Red Spectroscopry

Infra Red (IR) spectroscopy works by interrogating molecules with light. Molecular vibrations are quantised and so will absorb energy only in discrete packets. Most of these vibrations occur in the infrared region, and so certain wavelengths of IR radiation are absorbed. These form peaks, which can be related to the bonds of atoms, and thus molecular form.

The simplest form of IR is transmission. A sample is either pressed into a disc with KBr, which is transparent to IR, or supported in a beam using a holder transparent to IR radiation, usually in the form of a paste with nujol.

Transmission IR is a technique that focuses on the bulk of the sample, and as such is good for finding the structure of the catalyst studied, but not for the interaction of the catalyst with the gas molecules. Gas molecules adsorb on the surface, which is radically altered when a powdered sample is compressed into a disc. Diffuse Reflectance Spectroscopy (DRS) allows a powder to be used, as the sample is supported in a cup.

When a light beam encounters a surface, various interactions occur (Fig 2.1). The beam can be transmitted, reflected, absorbed or scattered. Transmission and reflection are elastic, in that energy is not converted. Absorption is an inelastic event, and scattering can be both. The section of interest is the inelastic scattering. A collimated IR beam is used to illuminate the sample. Most of the beam is reflected at the incident angle. This is known as specular reflection, and is generally useless, as it contains virtually all the radiation that has not interacted with the sample, giving the same output as input. The scattered light will come off at every angle, including the specular angle. The key to DRS is to maximise the non-specular signal with respect to the specular. DRS optics use parabolic reflectors with their foci on the sample to collect all the scattered radiation. This is then sent to the detector to recover the information from the interaction of light with the sample. As the ratio of the non-specular reflection to the incident IR beam is very low, a highly sensitive spectrometer must be used. A Fourier Transform (FT) spectrometer is ideal. When an FT spectrometer is used, as is common, the technique is know as Diffuse Reflectance Fourier Transform Spectroscopy or DRIFTS.

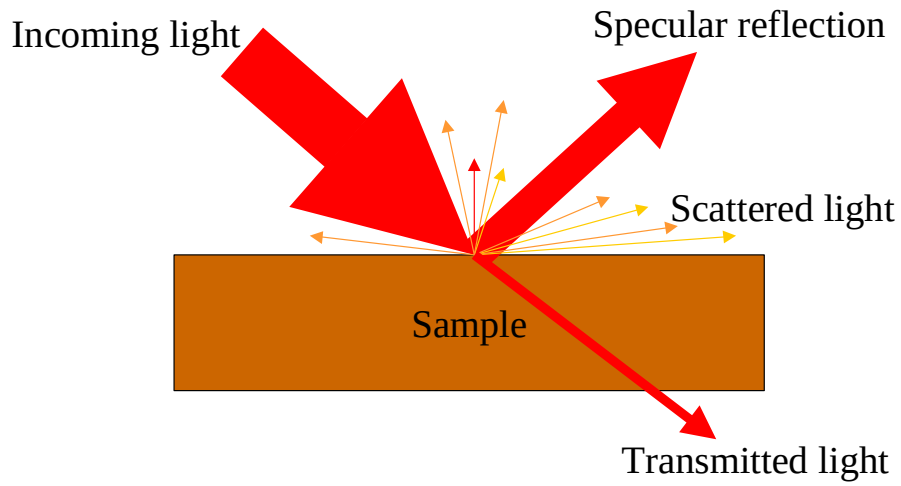

Fig 2.1: Interactions of light with matter

DRIFTS Experiments were carried out using a custom made cell [53] in DRIFTS optics supplied by Spectra-tech. The cell was designed to allow gas flow over the material being studied so that *in situ* measurements of the active catalyst could be taken. Its construction is detailed in Fig 2.2 below.

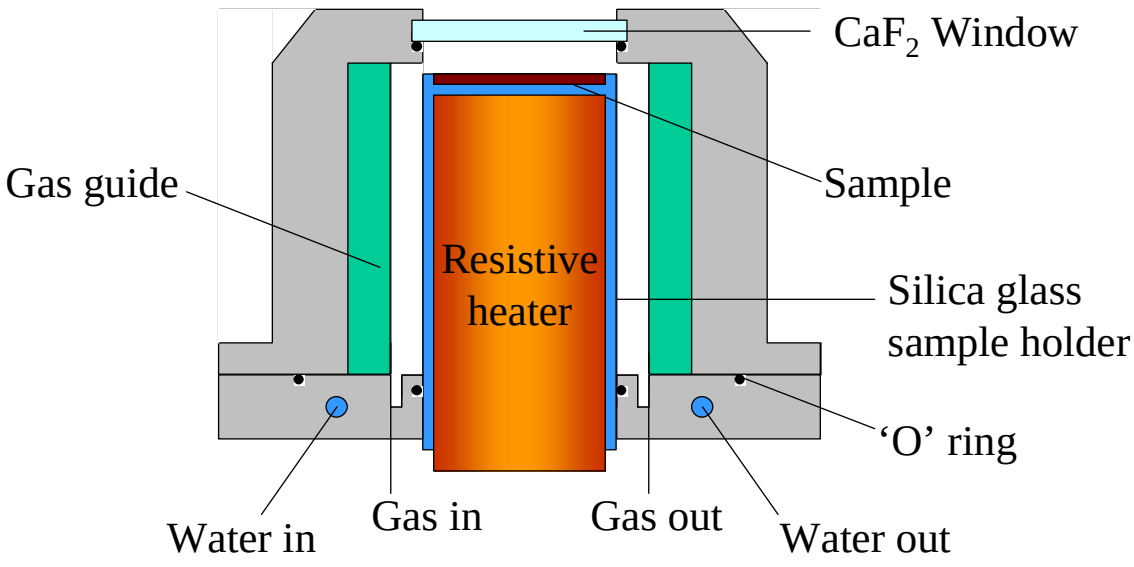

Fig 2.2: Custom made DRIFTS cell

In a typical DRIFTS experiment the catalyst was placed within the cell and purged under He. The non-specular radiation was optimised by manipulation of the mirrors and a background scan taken against which all other scans in the series were ratioed. This allowed for any difference in the spectrum due to a perturbation in the system to be easily seen. The perturbation applied to the system was the co-addition of CO to the He carrier gas flow. Adsorbed CO peaks could not be detected, so gas phase spectra obtained over the empty sample cup were subtracted from the sample spectra. A problem here is that it is very unlikely that spectra of the same intensity will be obtained. When subtracting a spectrum it is necessary to multiply the subtracted spectra by a coefficient to gain a sensible final spectrum. The value of the coefficient is of key importance in the effective use of this technique and must be optimised for every spectrum to cancel out the peaks of no interest whilst maintaining those which are being studied. However, this method is prone to the introduction of artefacts. Peaks that differ slightly can give rise to phenomenon that are a result of the subtraction, rather than those that are present due to the CO adsorbed. Gas supply to the cell was managed using MKS mass flow controllers and stainless steel Swagelok plumbing as detailed in Fig. 2.3. Helium was used as the carrier gas, and CO and O_2 were co-added to this stream. Research grade CO and O_2 were supplied by Linde gas, with He from BOC.

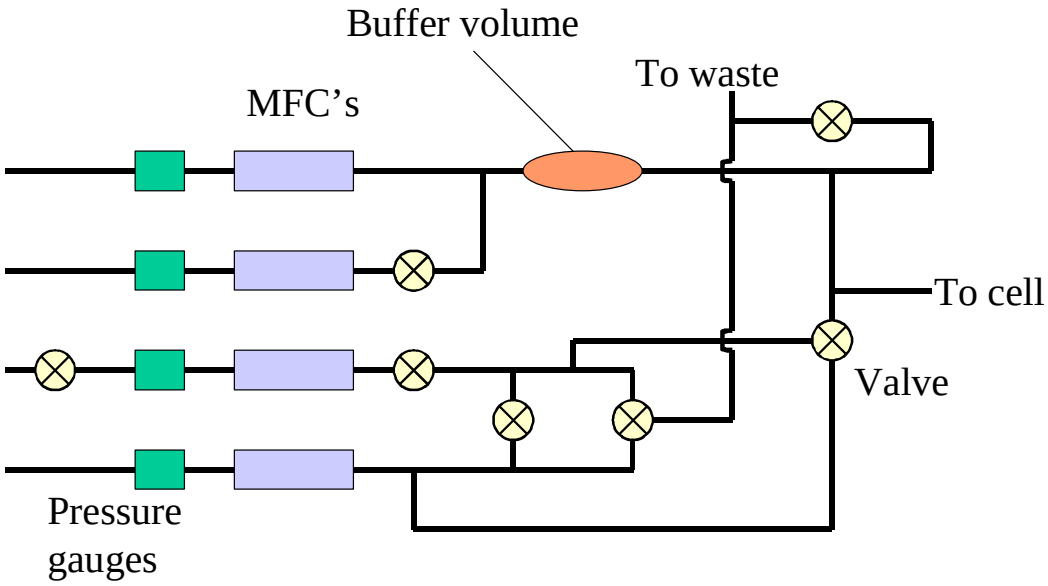

Fig 2.3: Gas handling apparatus for in-situ DRIFTS studies

2.2.3 Reactivity Studies

To test the activity of the various catalysts made, a ¼ inch outside diameter stainless steel tube reactor was used. Three Aera FC 7700C mass flow controllers, one each for He, CO and Oxygen regulated gas flow. These were connected via stainless steel 1/8 and 1/4 inch tubing with Swagelok connectors and controlled using an Aera ROD-4 controller to 47 ml min^{-1} He, 2 ml min^{-1} CO and 1 ml min^{-1} O_2.

The catalyst was first ground in an agate pestle and mortar, then approximately 100mg was taken and diluted in a 1:5 ratio with washed No.13 Ballotini (Glass beads 0.09-0.135mm diameter) to ensure even contact of the reactants with the catalyst. The mixture was placed between silica wool plugs in the reactor. The reactor was heated in an oven with a temperature controller, and the temperature was monitored using a thermocouple inserted into the catalyst plug. Measurements were taken using a Spectra Minilab LM80 Mass spectrometer. The arrangement of the apparatus is shown in Fig 2.4.

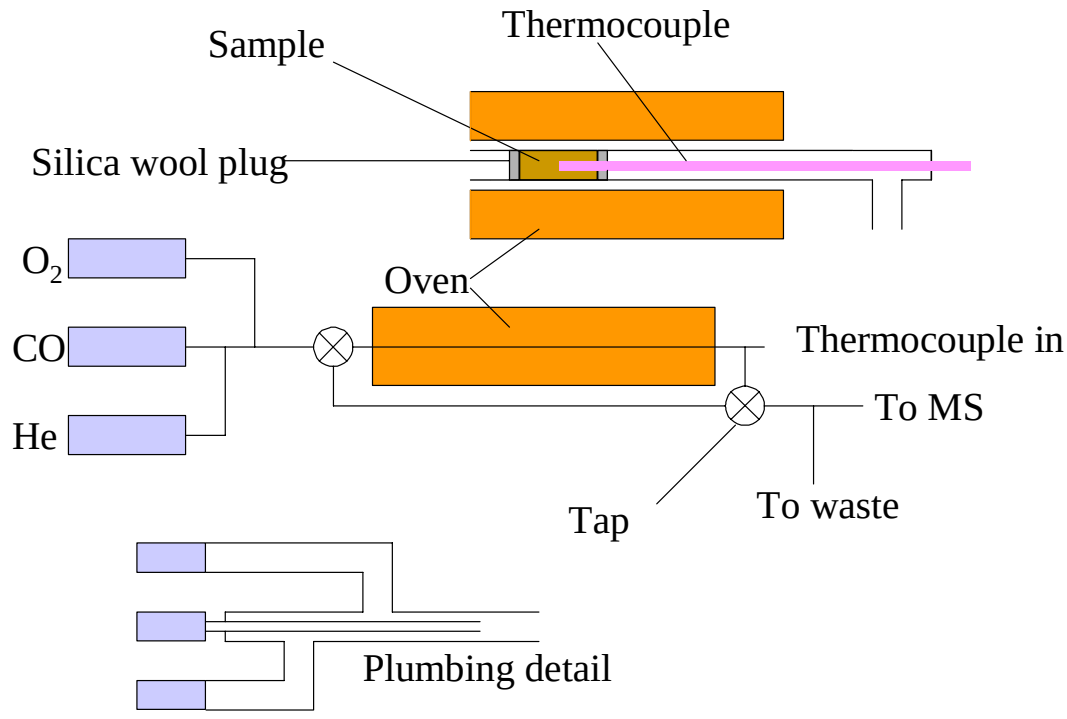

Fig 2.4: Apparatus used for determination of activity

Chapter 3: Results

3.1 Surface area

The BET surface areas of the various catalysts are given in Table 3.1.

Sample	Synthesis	BET Surface area (m^2/g)
Blank1	As-precipitated 1	54
Blank5	Combustion	39
Cat1	As-precipitated 1	37
Cat2	As-precipitated 1	119
Cat3	Combustion	48
Cat4	As-precipitated 2	134

Table 3.1:Surface areas of samples calculated by BET

The area of the catalysts varies over a significant range. The materials produced by combustion synthesis have uniformly low surface areas, whereas those produced by the as-precipitated method have more varying surface areas. Both Cat2 and Cat4 have anomalously high values.

3.2 X-ray diffraction

Powder X-ray diffraction patterns were taken for every sample and are shown below with reference data in Fig. 3.1 and Fig. 3.2. The peaks shown on Cat4 at 38.2°, 44.5° and 64.7° are solely those due to the presence of gold particles.

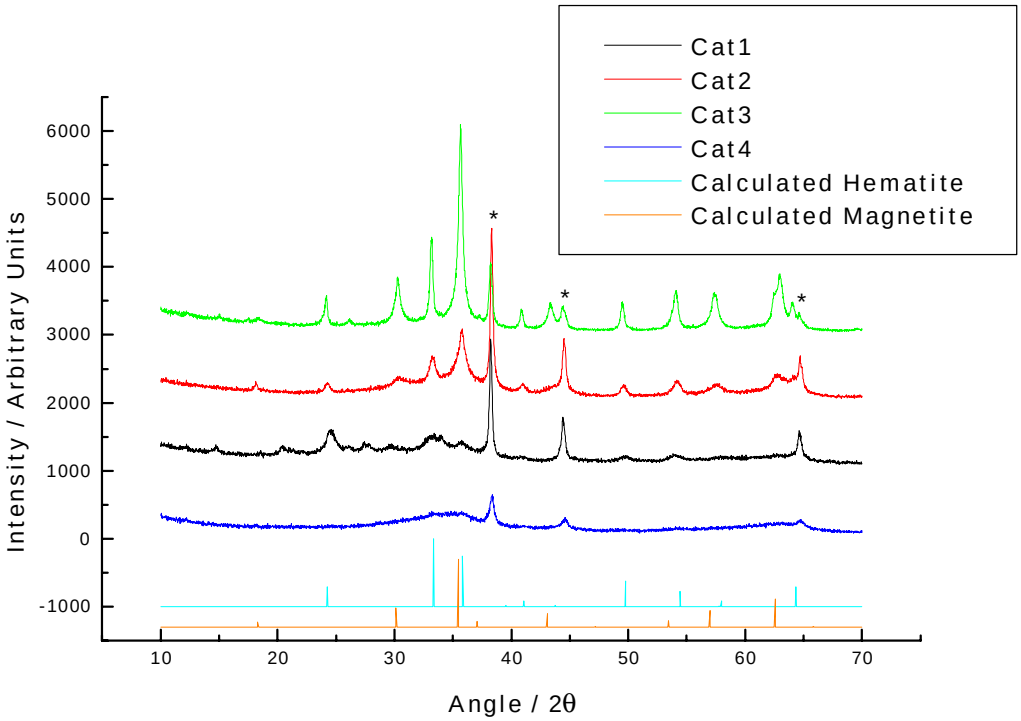

Fig. 3.1: Powder XRD patterns for catalysts and reference. Gold peaks marked with asterisk

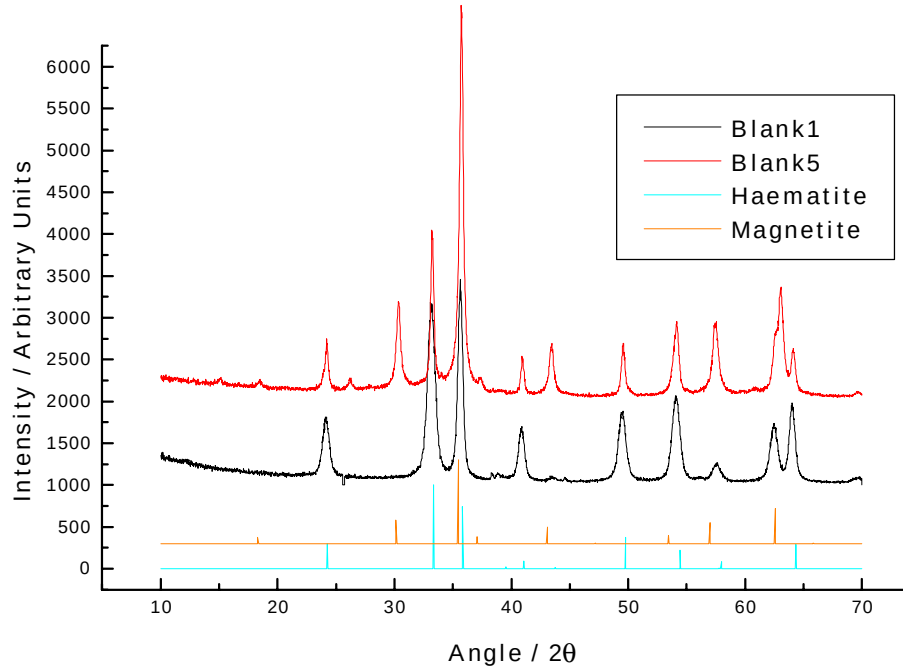

Fig. 3.2: Powder XRD patterns of blank samples and reference

The peaks due to gold can be seen on all the other catalysts as well. Most peaks present on the patterns of the other catalysts are assigned to haematite and either magnetite or γ-Fe_2O_3. As magnetite and γ-Fe_2O_3 have very similar diffraction patterns, a definitive assignation is not possible. From the quality of the peaks it is possible to infer the relative crystallinity of the support material. Cat4 has the least crystalline support, as the peaks are so broad as to be indistinguishable. Cat3 has the sharpest peaks and therefore the most crystalline support. Cat2 appears to be more crystalline than Cat1.

XRD of the blank samples was undertaken to check that the same support phases were produced, but also to ensure that the peaks attributed to gold were assigned correctly. Aluminium has a very similar diffraction pattern to gold and aluminium sample holders were used to take the XRD patterns. If the X-rays penetrated the samples, peaks due to aluminium would be visible. Fig. 3.3 shows that the peaks due to the blank samples do not correspond with the Al peaks and that in normal use, the X-rays do not penetrate the sample.

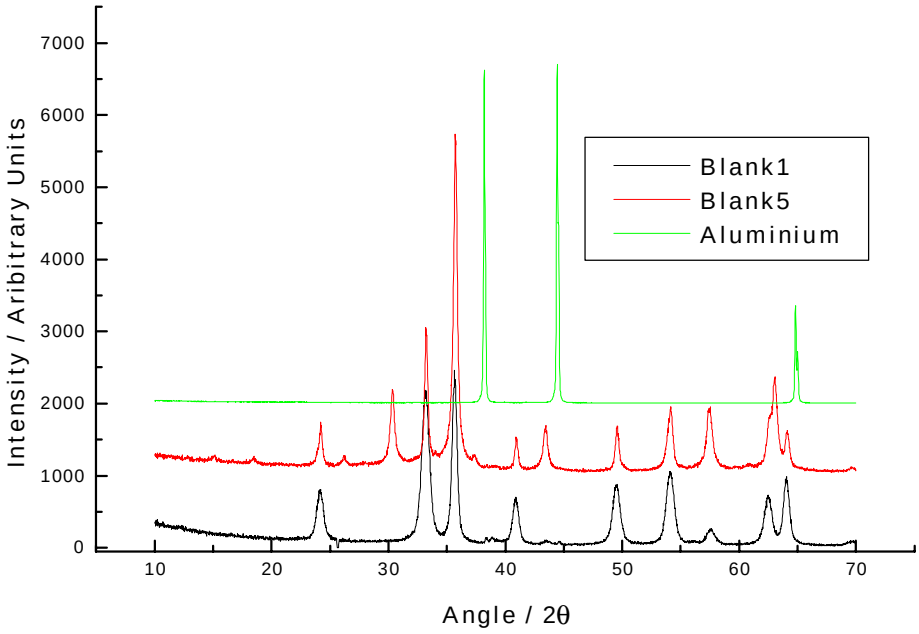

Fig. 3.3: Powder XRD patterns of blank samples and Al sample holder

3.2.1 Particle size using Scherrer equation

The mean gold crystallite size was estimated using the XRD peaks at 38.2° and 44.5° for each of the catalysts, assuming that the particles were spherical. The results are tabulated in Table 3.2

Sample	Synthesis	Size/nm from 38.2° peak	Size/nm from 44.5° peak	Size/nm average
Cat1	As-precipitated 1	54	88	71
Cat2	As-precipitated 1	153	125	139
Cat3	Combustion	71	77	74
Cat4	As-precipitated 2	48	35	42

Table 3.2: Gold particle size from calculations using the Scherrer equation

3.2.2 Single crystal X-ray diffraction

A single crystal of triphenylphosphine gold nitrate, synthesised at the same time as that used in Cat4, was submitted for unit cell analysis. This agreed with literature sources [54]. The analysis of a synthesised $AuPPh_3NO_3$ crystal showed that the synthesis, although giving low yields, was producing the required product.

3.3 Microscopy

3.3.1 TEM

Transmission electron microscopy showed a varied morphology of the catalysts produced. As the aim of this technique was to gauge the size of the gold particles, the blank samples were not studied. No particles were found on Cat3 that could be categorically assigned to gold. The average particle size is given in Table 3.3 below, and the distribution of gold sizes is displayed in Fig. 3.4.

Sample	Synthesis	Particles counted	Average particle size / nm
Cat1	As-precipitated 1	25	29.7
Cat2	As-precipitated 1	165	14.0
Cat3	Combustion	N/A	N/A
Cat4	As-precipitated 2	44	18.7

Table 3.3: Gold mean particle size from TEM micrographs

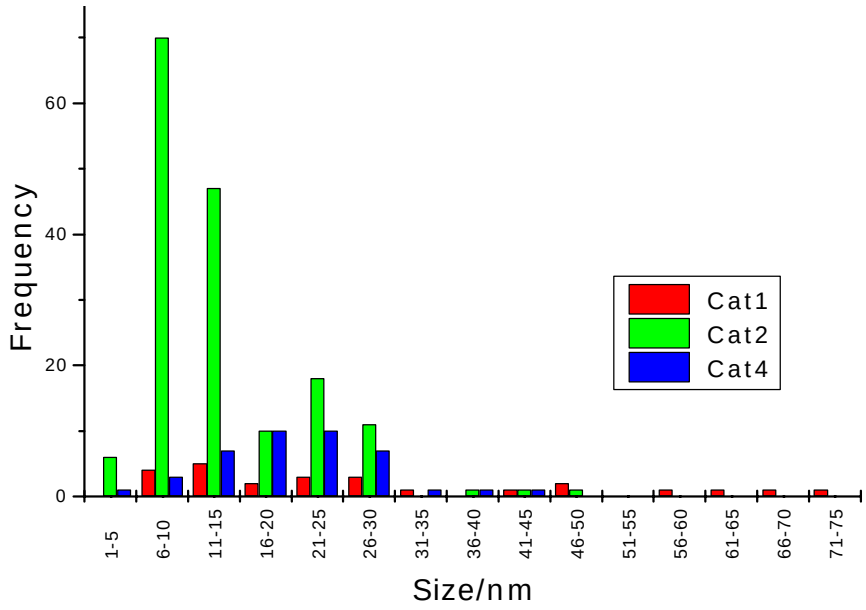

Fig. 3.4: Histogram of gold particle sizes as measured from TEM micrographs

Cat1 showed a fairly even coverage of gold particles throughout the support, as can be seen in Fig. 3.5. Arrows indicate gold particles.

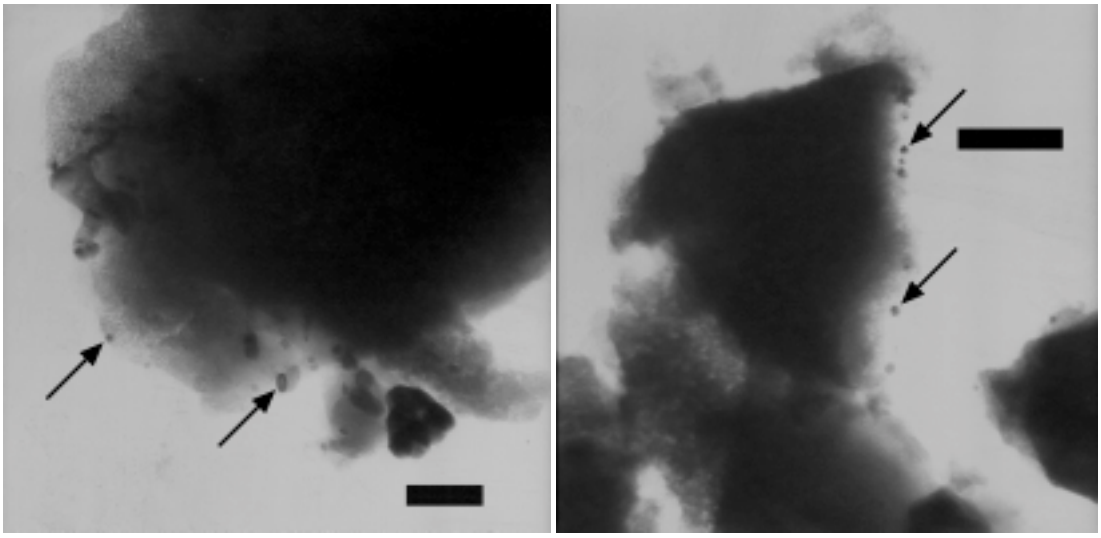

a *b*

Fig. 3.5: TEM micrographs of Cat1; a) bar shows 100nm, b) bar shows 200nm

Cat2 showed a more uneven coverage (Fig. 3.6). The gold particles were clustered together, so that areas of the support showed very few particles (c), and other parts had a high concentration (a). Arrows used to identify gold particles. Note agglomerated gold particles shown in a.

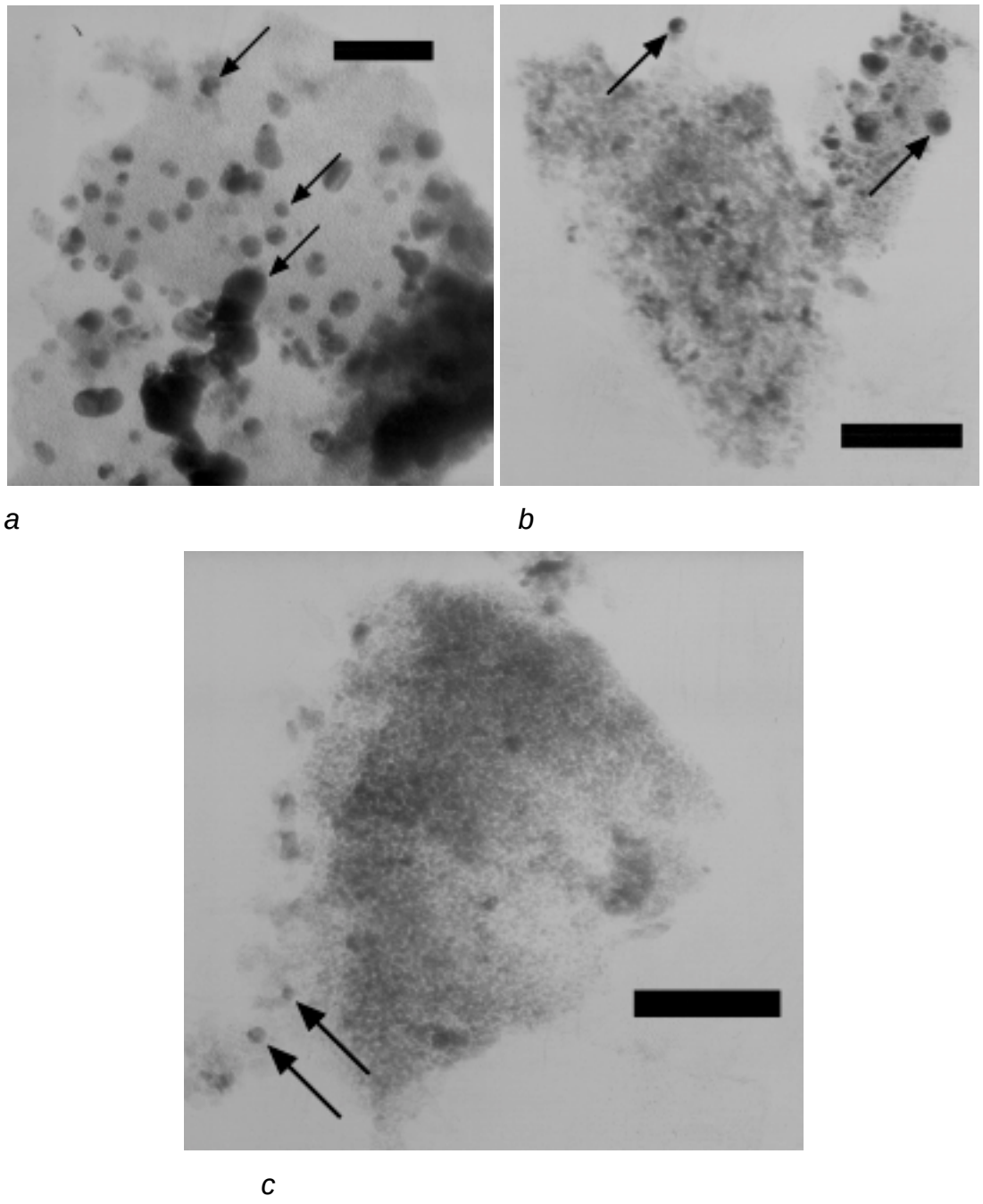

Fig. 3.6: TEM micrographs of Cat2; bar shows 100nm in each case

Cat3 showed a very different support morphology to the as-precipitated catalysts. Where the as-precipitated catalysts showed a fairly evenly support illumination, the combustion synthesised support seemed to have a morphology similar to screwed-up tissue paper. Cat3 also lacked particles that could be categorically identified as gold with this method (Fig. 3.7). Areas that appeared to contain gold at lower magnification revealed that they did not when at higher magnification.

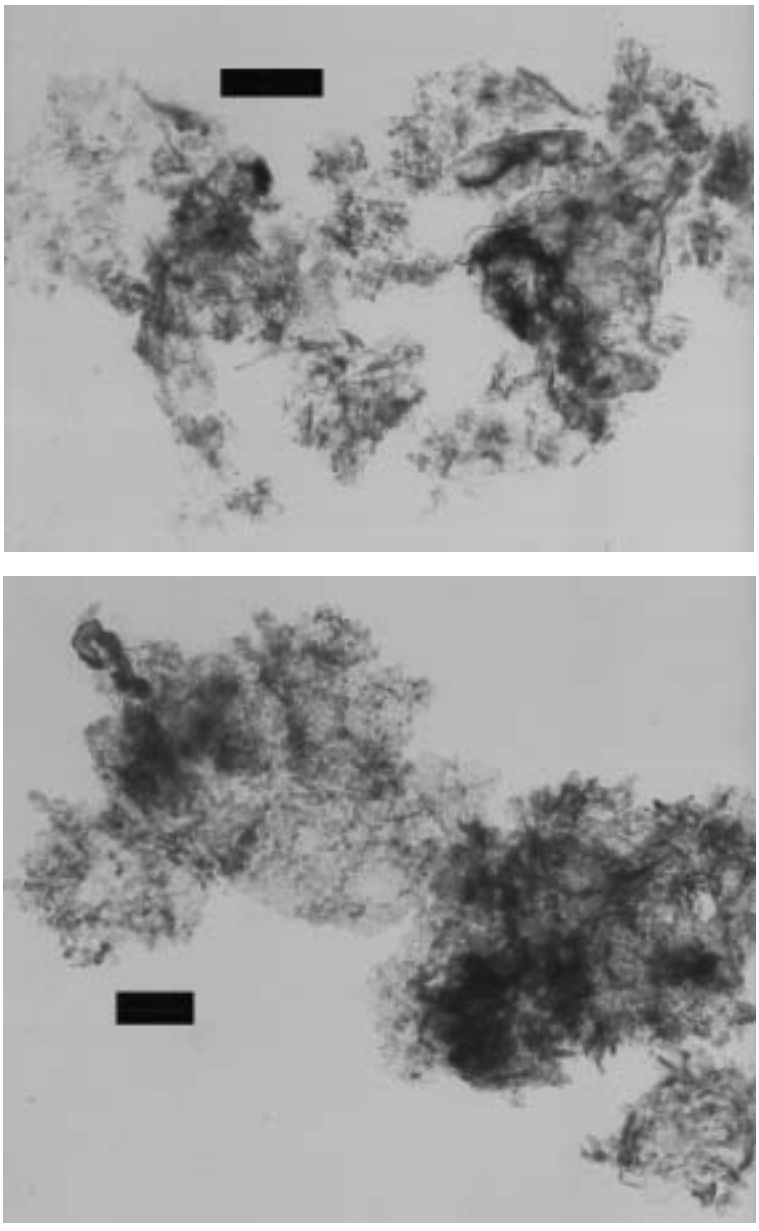

Fig. 3.7 TEM micrographs of Cat3; a) bar shows 500nm, b) bar shows 200nm

Fig. 3.8 shows representative TEM micrographs for Cat4. Gold was evenly dispersed across most images.

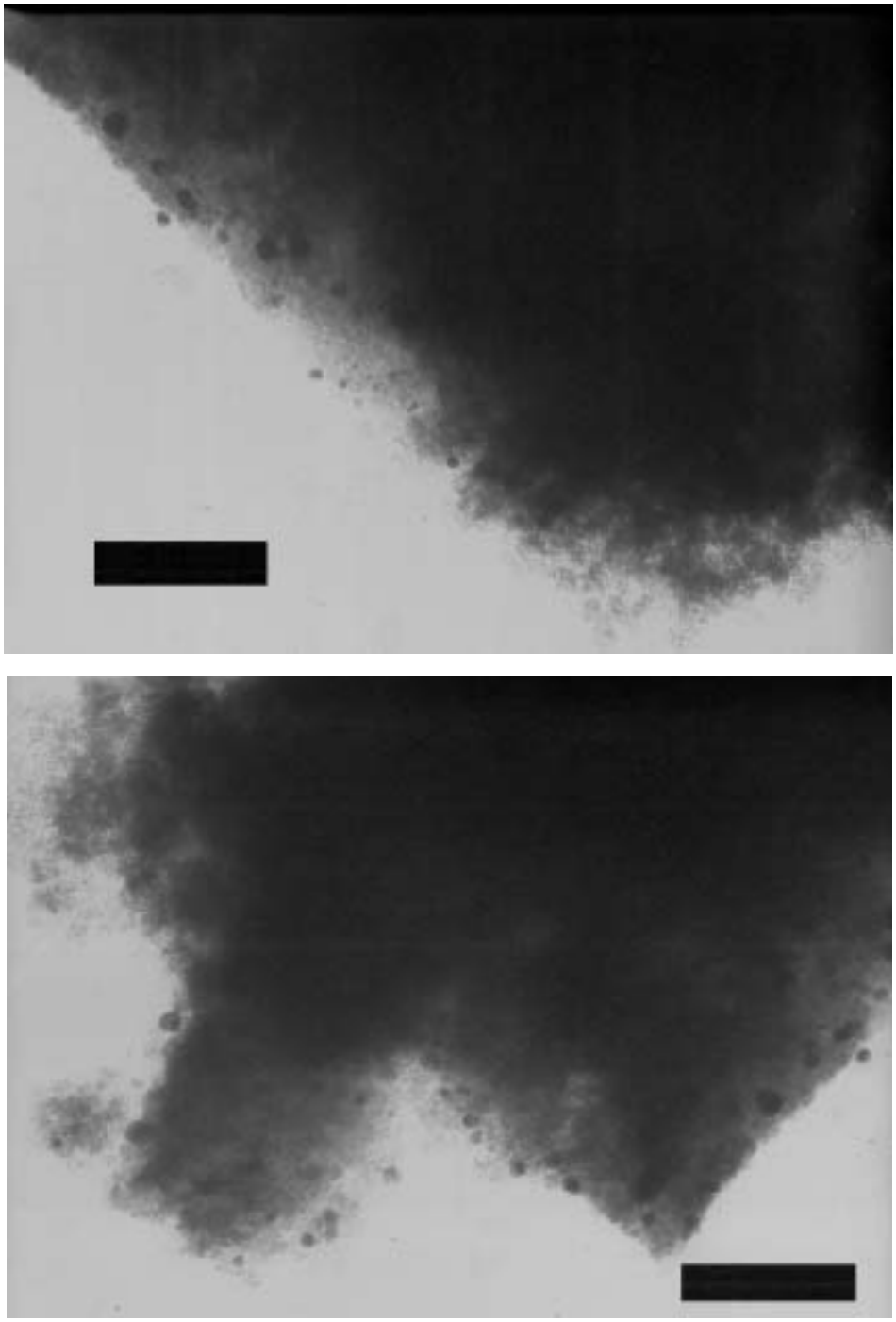

Fig. 3.8 TEM micrographs of Cat4. Bar shows 200nm in each case

The TEM does not show evidence for the shape of the gold particles being hemispherical, as reported by Haruta [55]. Instead, they appear as spheres for the most part, although agglomeration has also produced some large irregular structures as shown in Fig 3.6 a.

3.3.2 SEM

Secondary electron detector micrographs of all of the samples showed a rough support morphology with a wide range of particle sizes (Figs. 3.9-3.14).

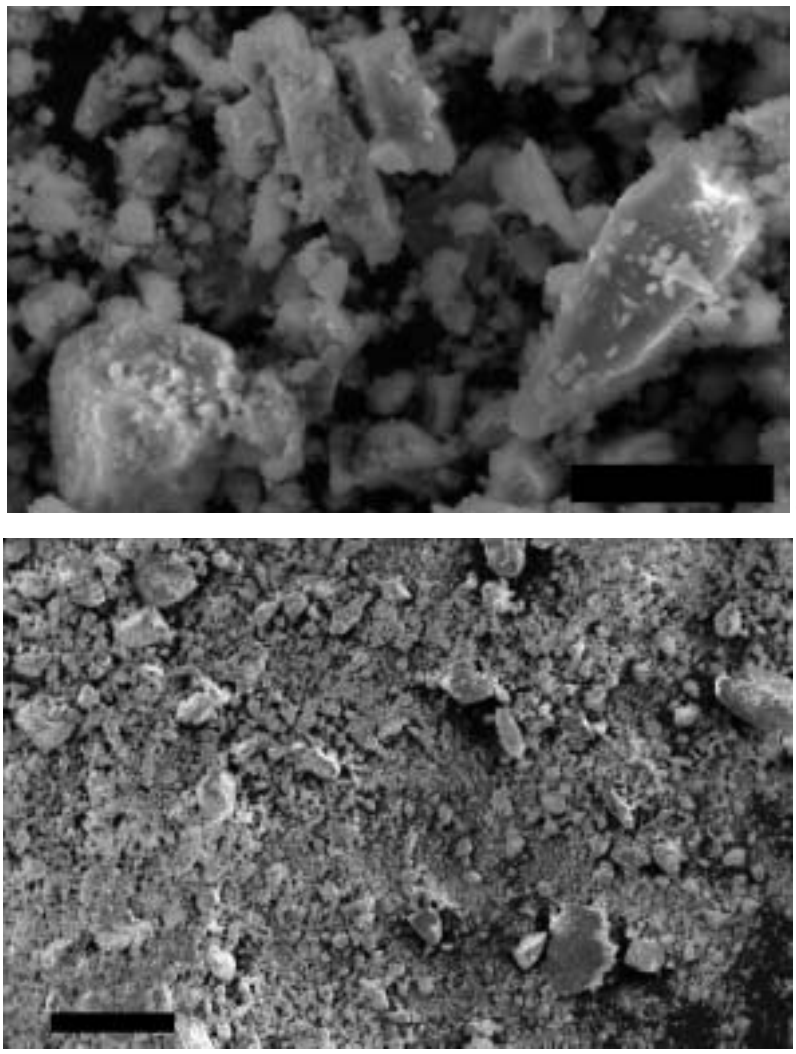

Fig. 3.9 Secondary electron SEM micrographs of Blank1; a) bar shows 20μm, b) bar shows 500μm

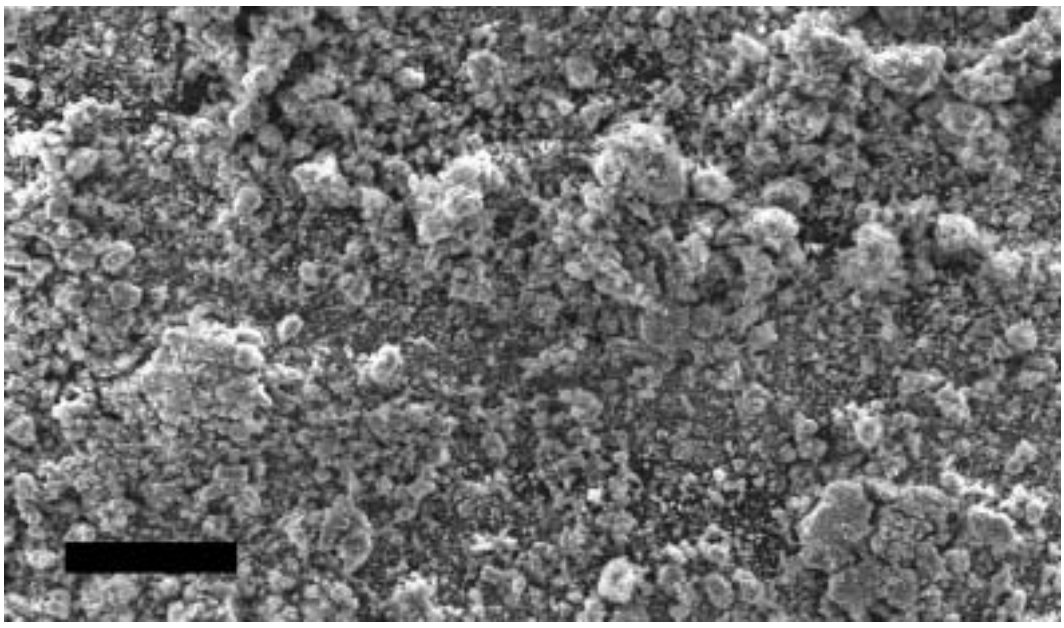

a

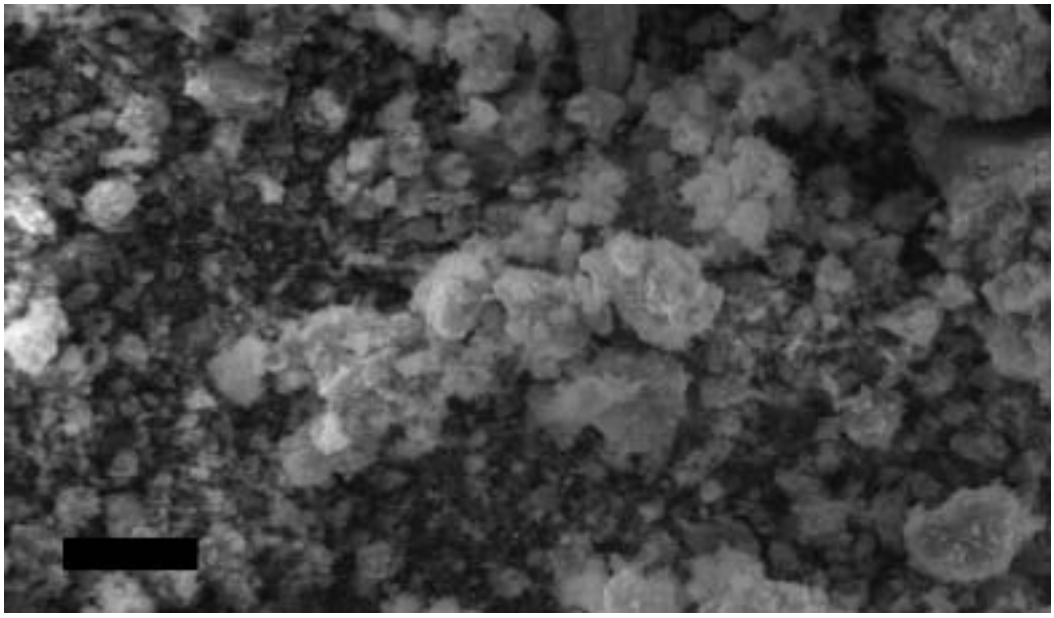

b

Fig. 3.10: Secondary electron SEM micrographs of Blank5; a) bar shows 200μm, b) bar shows 20μm

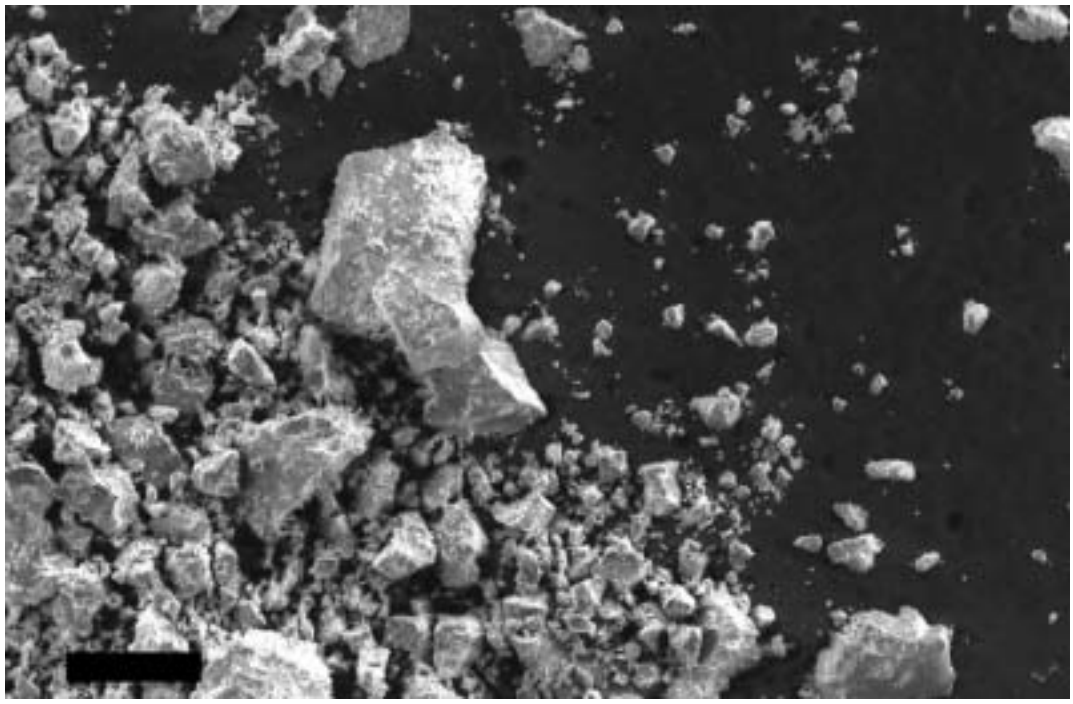

a

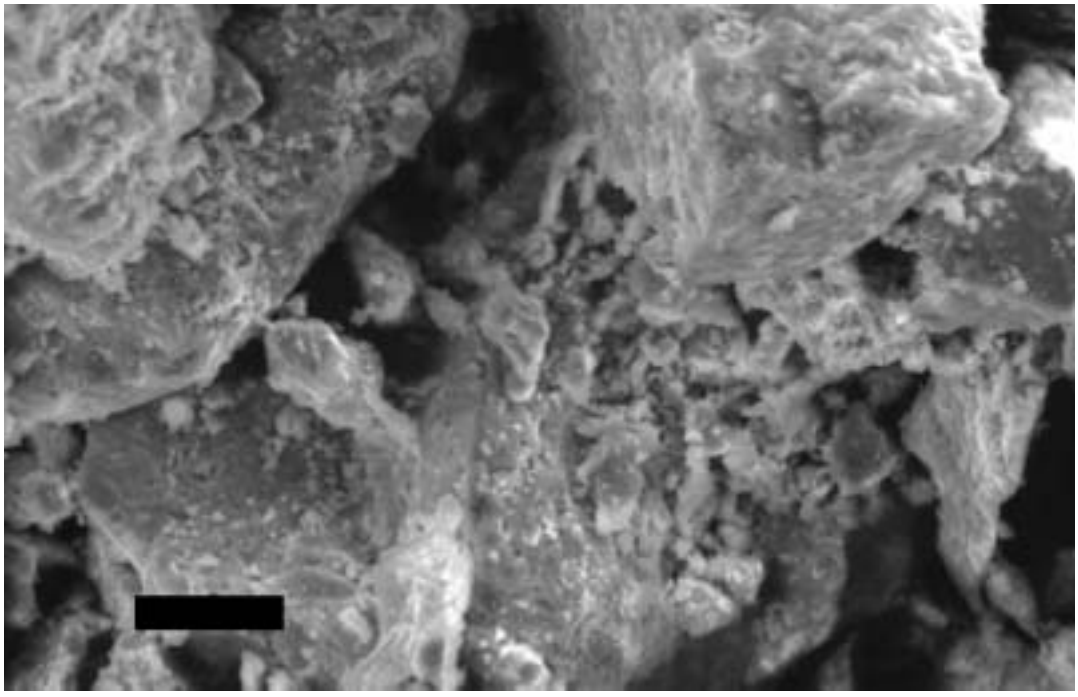

b

Fig. 3.11: Secondary electron SEM micrographs of Cat1; a) bar shows 200μm, b) bar shows 20μm

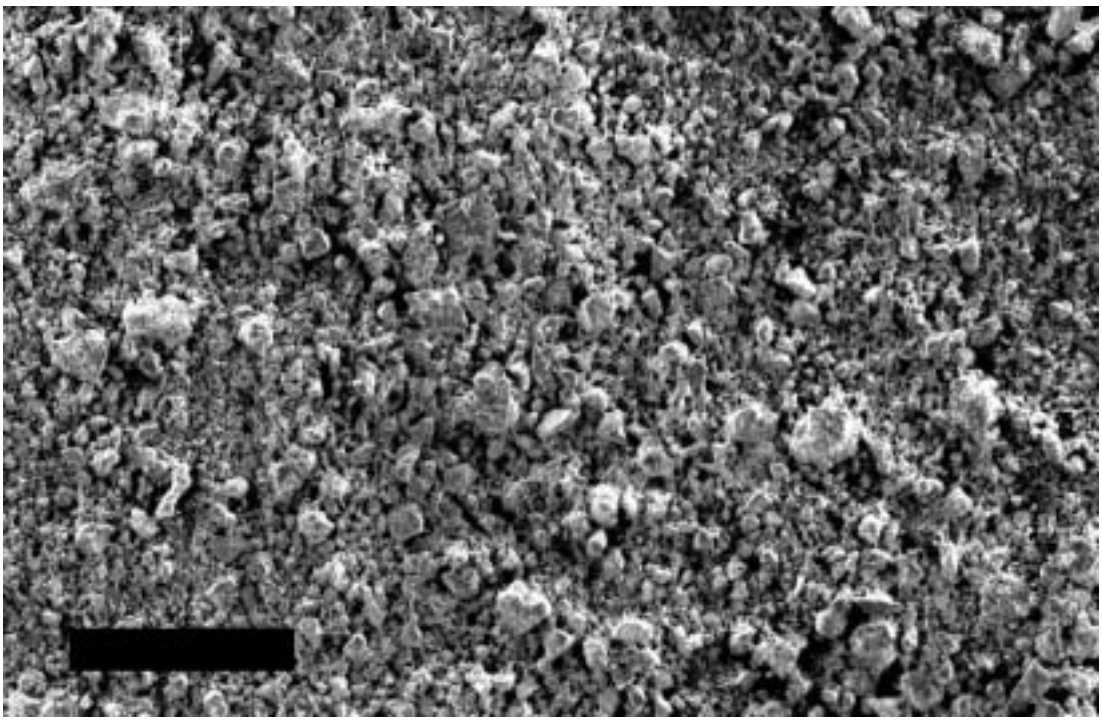

Fig. 3.12: Secondary electron SEM micrograph of Cat2; bar shows 500μm

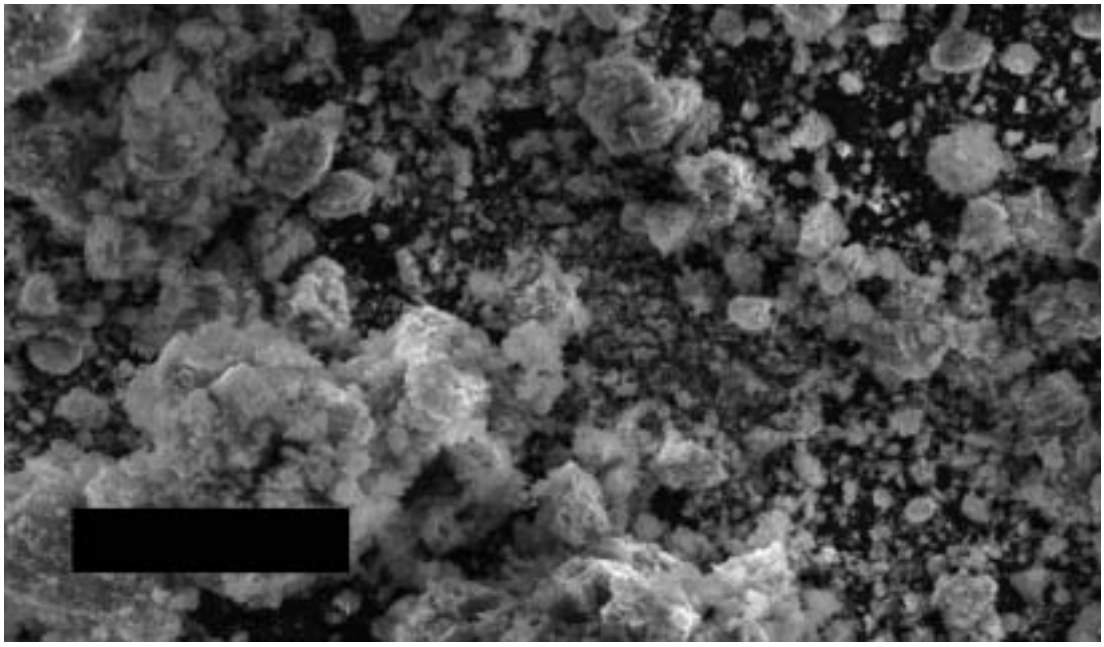

Fig. 3.13: Secondary electron SEM micrograph of Cat3; bar shows 100μm

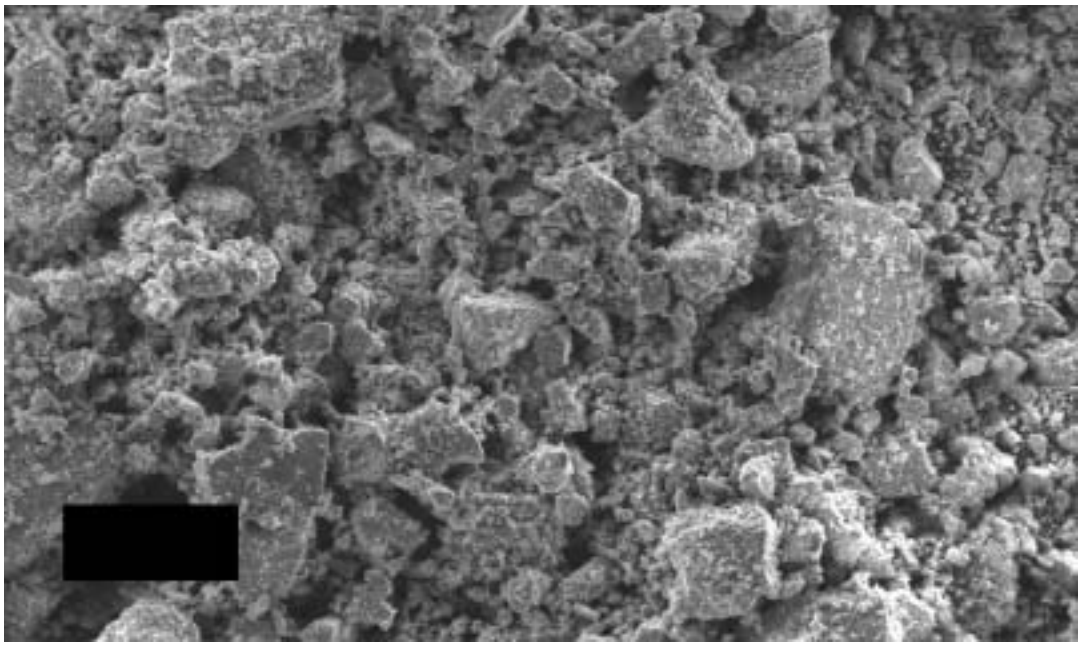

a

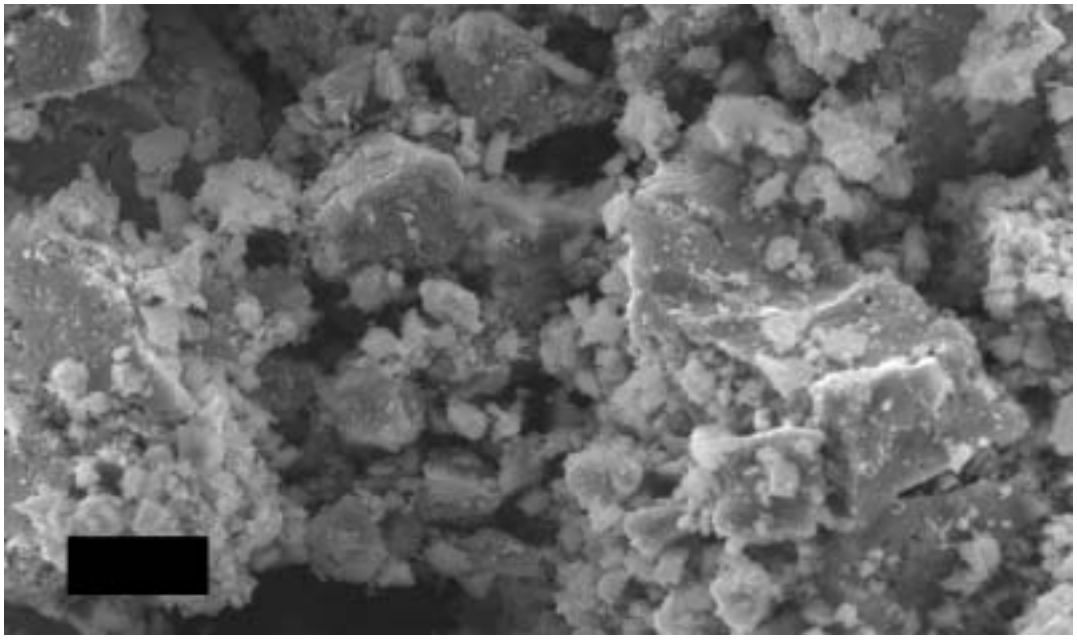

b

Fig. 3.14: Secondary electron SEM micrographs of Cat4; a) bar shows 200μm, b) bar shows 20μm

The back-scattering detector shows Cat1 with a large number of well-dispersed gold particles (Fig. 3.15), whereas Cat2 appears to have a much greater number of irregular large particles (Fig. 3.16), but shows a number of smaller particles at high magnification as well. Cat 3 also shows this pattern, but has fewer particles which are somewhere between the two sizes (Fig. 3.17). Cat 4 at low magnification does not appear to have many gold particles at all, but at much higher magnification, shows some smaller particles with poor resolution, indicated with arrows (Fig. 3.18).

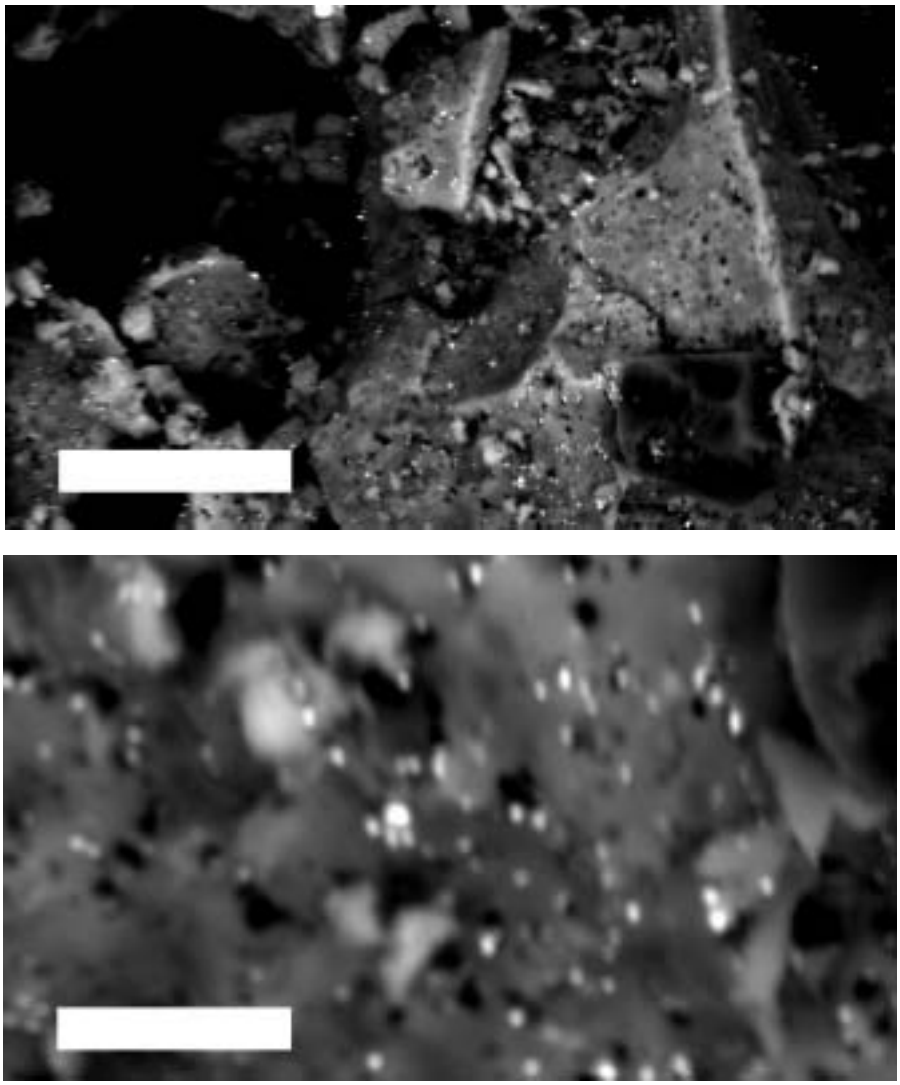

Fig. 3.15: Back-scattered electron SEM micrographs for Cat1; a) Bar shows 20μm, b) bar shows 5μm

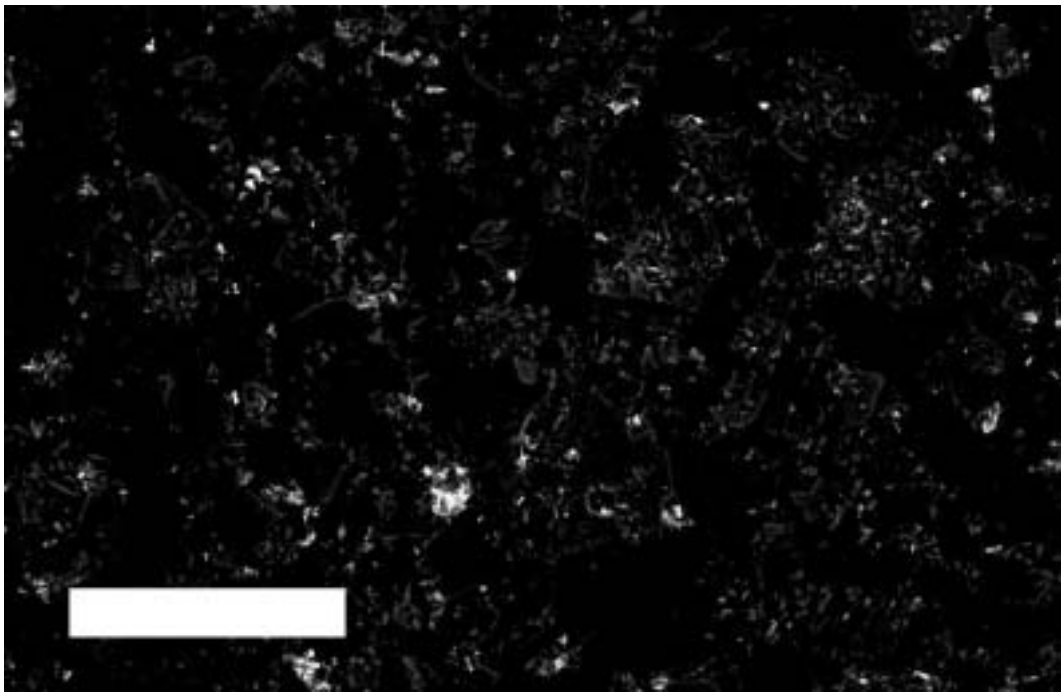

a

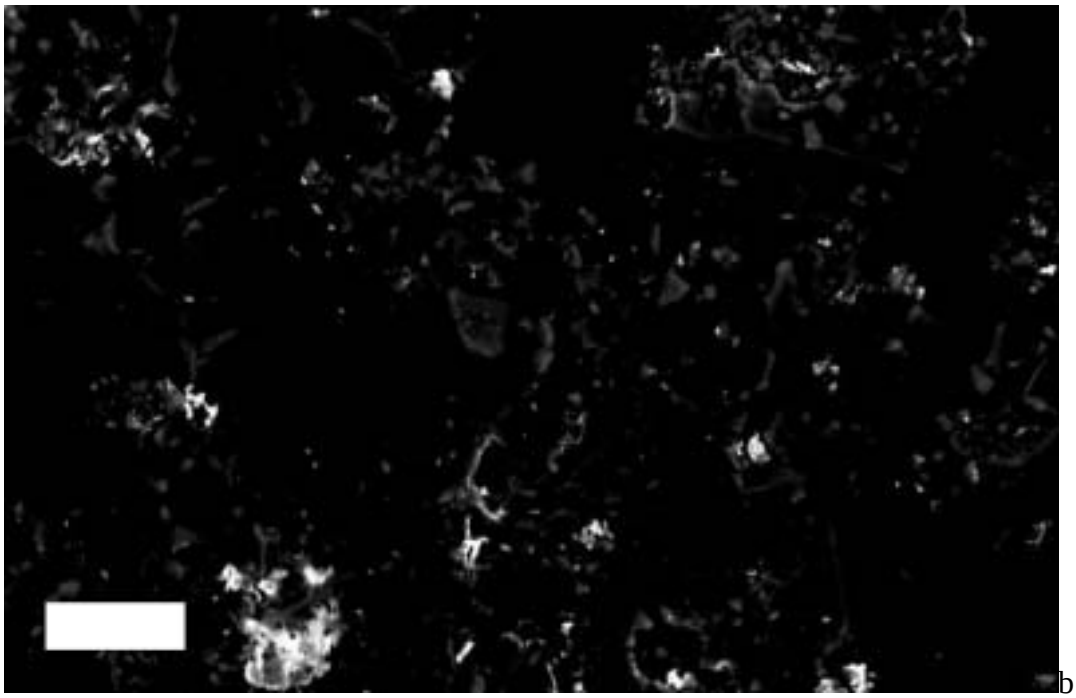

b

Fig. 3.16: Back-scattered electron SEM micrographs for Cat2; a) Bar shows 100μm, b) bar shows 20μm

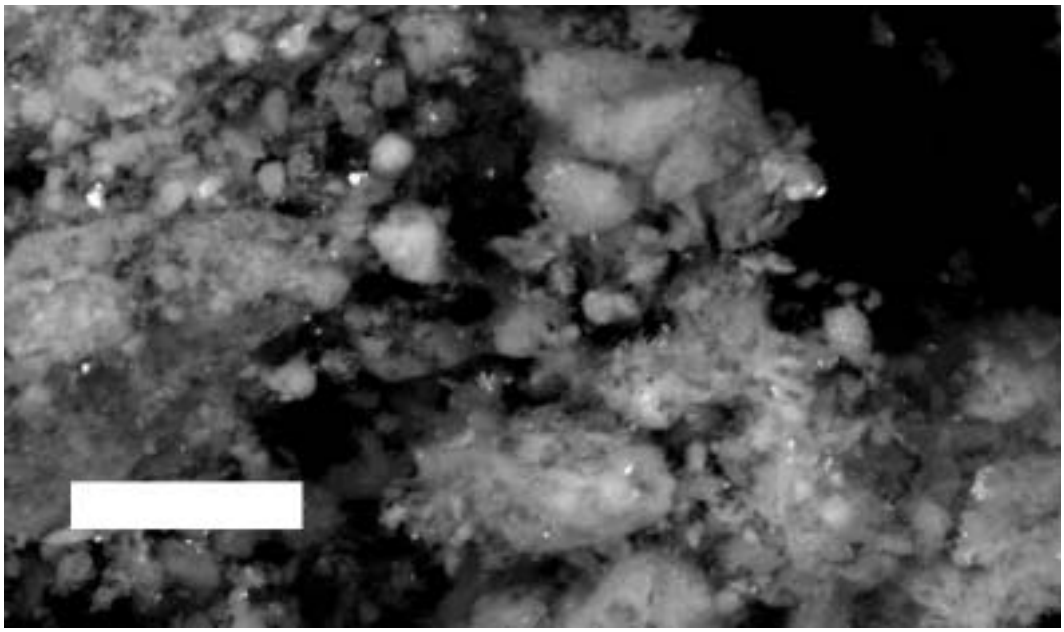
a

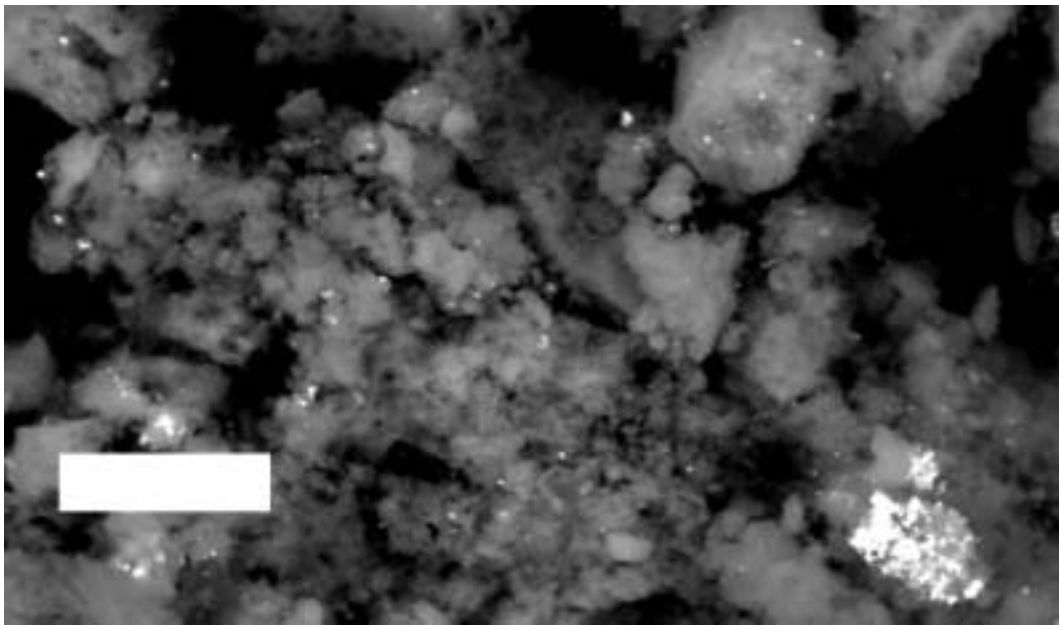
b

Fig. 3.17: Back-scattered electron SEM micrographs for Cat3; a) Bar shows 20μm, b) bar shows 10μm

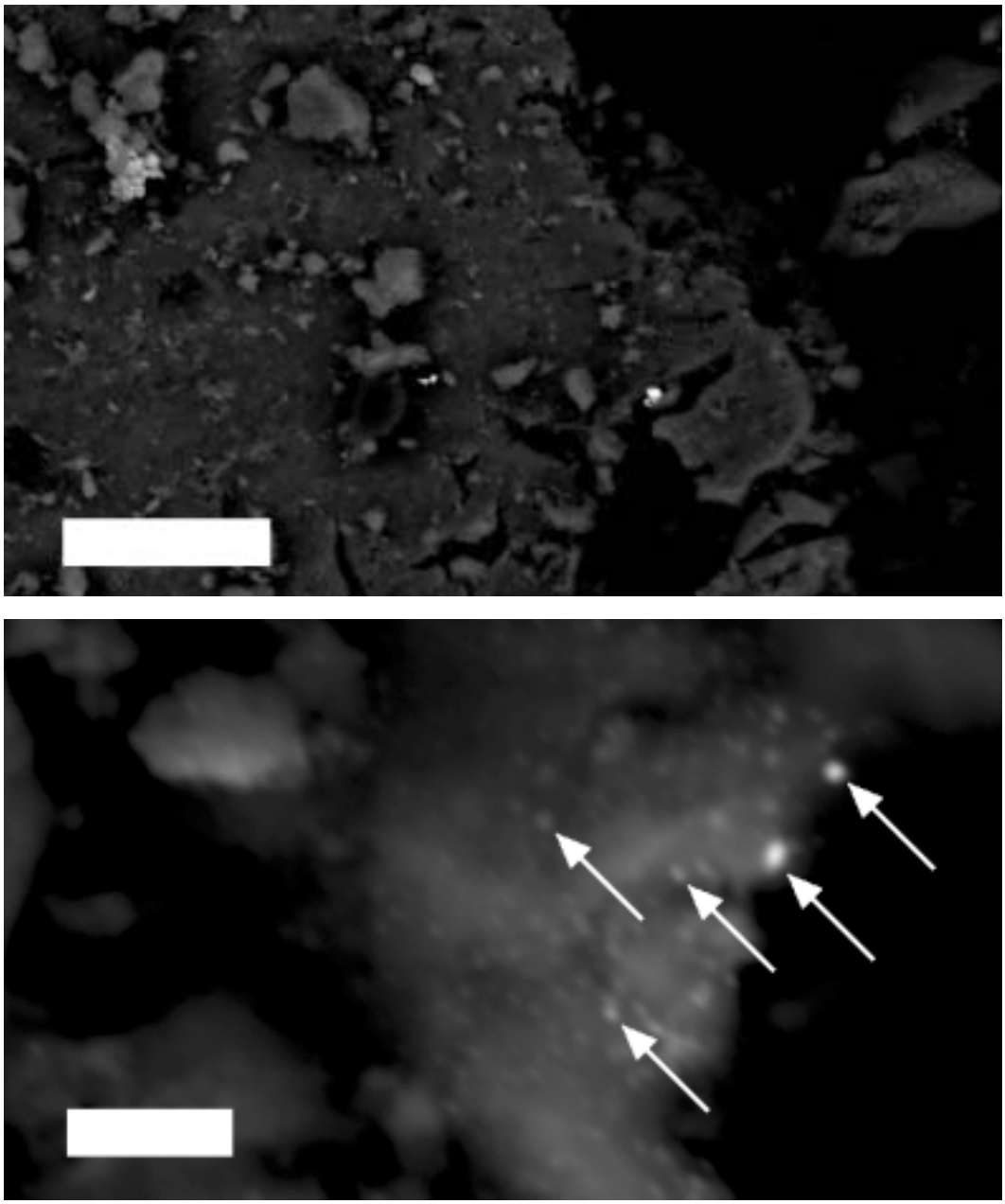

Fig. 3.18: Back-scattered electron SEM micrographs for Cat4; a) Bar shows 20μm, b) bar shows 2μm

3.3.3 EDS

Fig. 3.19 shows the EDS spectrum of the blank adhesive carbon disc used for mounting samples in the SEM and EDS instrument. The results for the samples are detailed in figs. 3.20 and 3.21.

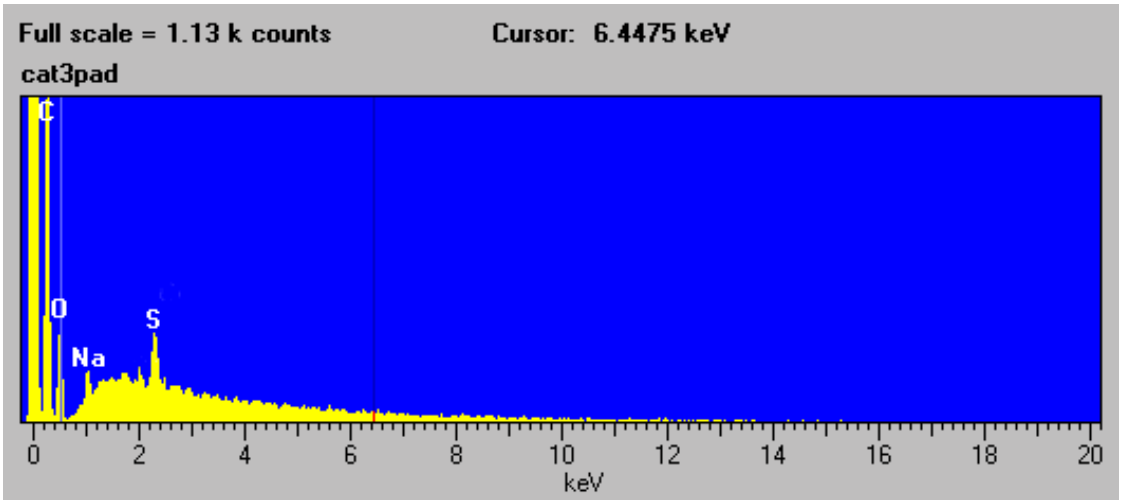

Fig. 3.19: EDS spectrum of adhesive carbon pad used to mount samples in SEM and EDS instrument

Cat1 and Cat2 show the presence of iron, oxygen and gold, as expected, although Cat2 also has significant quantities of silicon. Cat3 shows iron, oxygen, gold and chlorine are present, whilst Cat4 shows iron, oxygen, gold and silicon. Blank1 shows iron, oxygen and sodium, although Blank5 only shows iron and oxygen. The distribution of these elements is presented in Table 3.4.

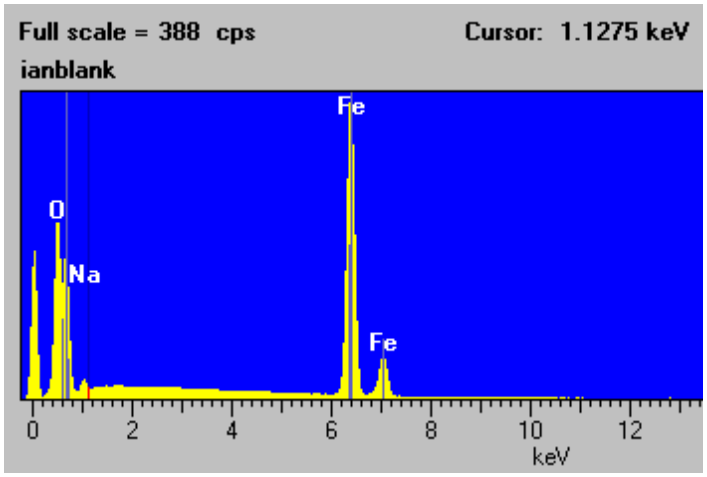

a

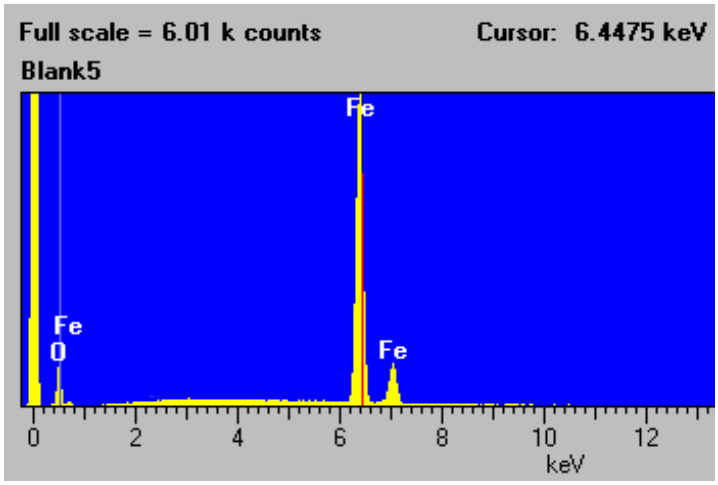

b

Fig. 3.20 EDS spectra for the blank samples; a) Blank1, b) Blank5

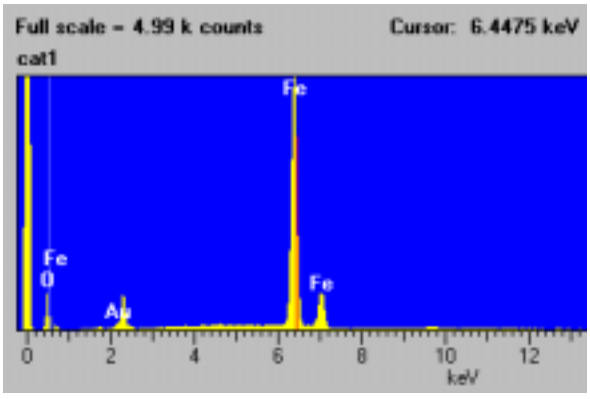

a

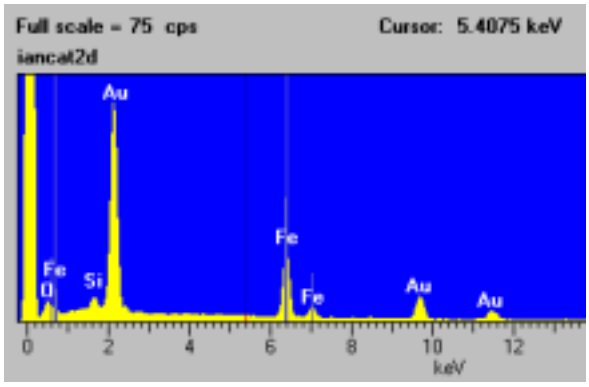

b

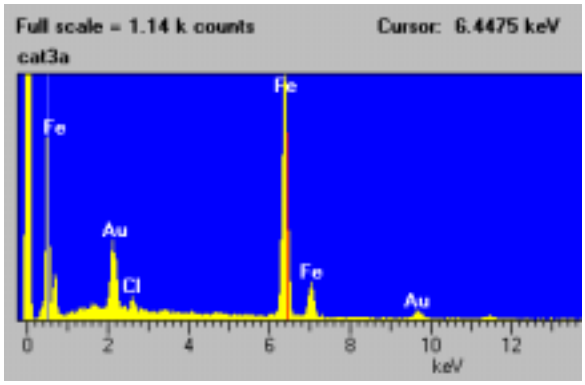

c

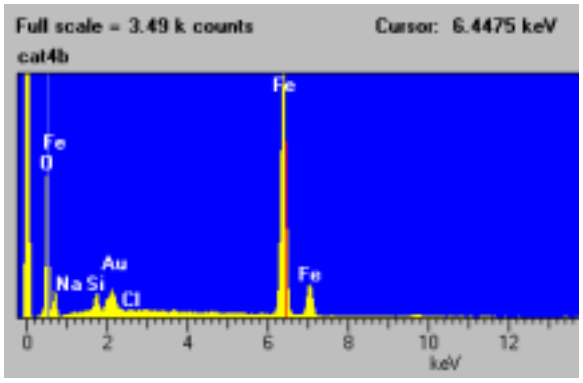

d

Fig. 3.21: EDS spectra for gold containing samples; a) Cat1, b) Cat2, c) Cat3, d) Cat4

Sample	Elements detected by EDS							
	Iron	Oxygen	Gold	Silicon	Sodium	Chlorine	Carbon	Sulfur
Empty Pad		X			X		X	X
Blank1	X	X			X			
Blank5	X	X						
Cat1	X	X	X					
Cat2	X	X	X	X				
Cat3	X	X	X			X		
Cat4	X	X	X	X				

Table 3.4: Summary of elements detected by EDS

3.4 XPS

Survey scans of all samples were taken, along with more detailed spectra in the Au 4d, Au 4f, Fe 2p and P2p regions. Resolution was 0.5eV for the survey scans and 0.1 eV for all other spectra. All spectra obtained were corrected to the carbon peak at 285 eV before any interpretation was begun. The spectra are displayed in Figs. 3.22-3.26 below.

The survey scans show three minor variations between the samples which are worthy of note before offering a more detailed explanation of the major features. On Blank1 are features at 494 and 1072 eV not present on the other samples (a and c in Fig. 3.22). These can be assigned to Sn 3d3 and Na 1s respectively. The other feature is at 686 eV and appears on Cat2 and Cat4. This was assigned to the F 1s. Otherwise, there is reasonable consistency between the various sample and reference spectra with the remaining peaks associated with the anticipated elements.

Fig. 3.23 shows the Au 4d region and indicates the presence of gold in the as-precipitated catalysts, but not in Cat3, or the blanks. Fig. 3.24 shows the spectra for the Au 4f region for the catalysts, indicating the same. In this region however, the peak positions vary. Cat1 shows peaks at 84 and 87 eV, but these are shifted to 85 and 89 eV for Cat2 and Cat4. The peaks for Cat2 and Cat4 also appear to have shoulders corresponding to the peak positions from Cat1.

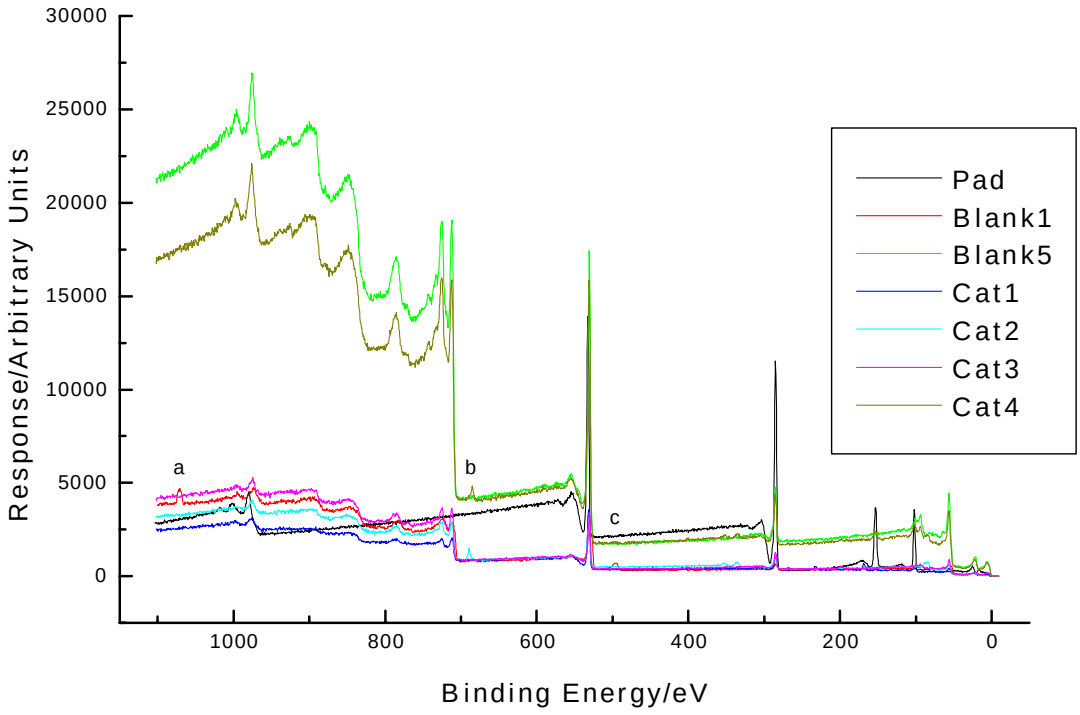

Fig. 3.22: XPS survey spectra for all samples

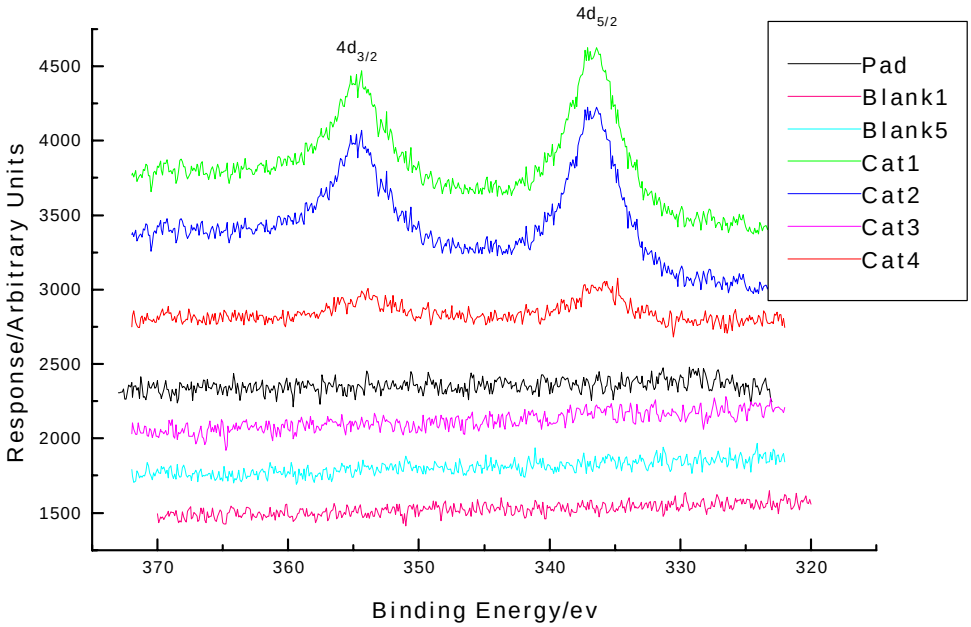

Fig. 3.23: XPS spectra for all samples in the Au 4d region.

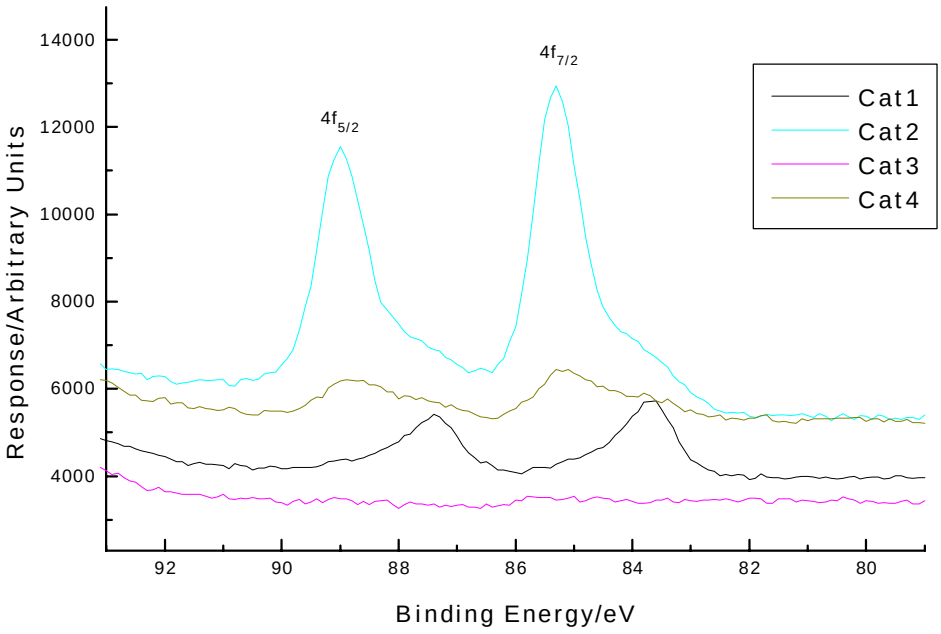

Fig. 3.24: XPS spectra for the catalysts in the Au 4f region

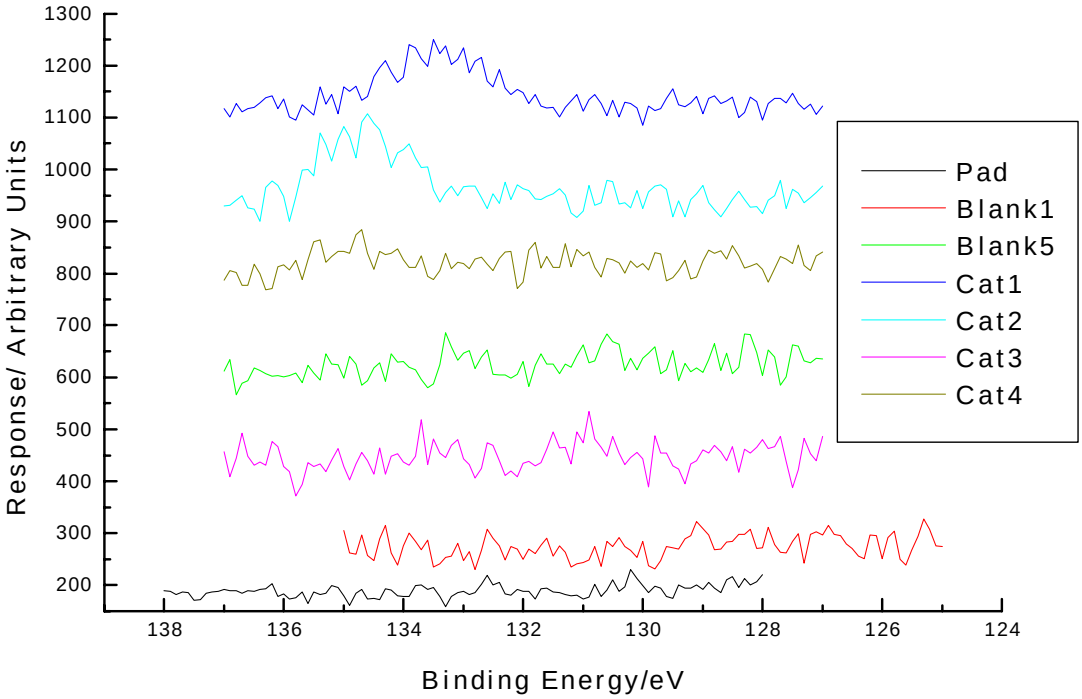

Fig. 3.25: XPS spectra for all samples in the P 2p region

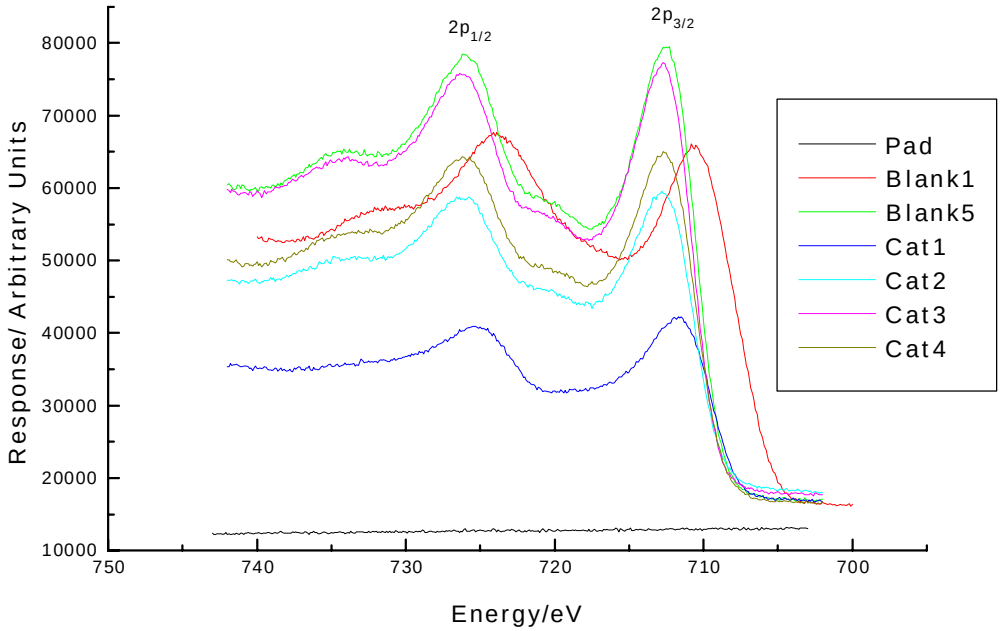

Fig. 3.26: XPS spectra for all samples in the Fe 2p region

The XPS of the P 2p region shows that phosphorus residue is only present in Cat1 and Cat2. The amount of noise in the spectra shows that it is only present in low quantities.

The XPS for the Fe 2p region is shown in Fig. 3.26. All of the samples show a similar spectrum for the Fe 2p region, except Blank1 and Cat1. Where all of the other materials have peaks at 726.1 and 712.6 eV, Blank1 has peaks shifted to 724.0 and 710.7 eV. Cat1 has peaks at 725.4 and 711.6 eV. A satellite peak between these two peaks is much more prominent on the samples with higher binding energies.

3.5 IR spectroscopy

Fig. 3.27 shows the DRIFTS spectra obtained for the catalysts under CO, and Fig. 3.28 shows the corresponding spectra after subtraction of the gas phase

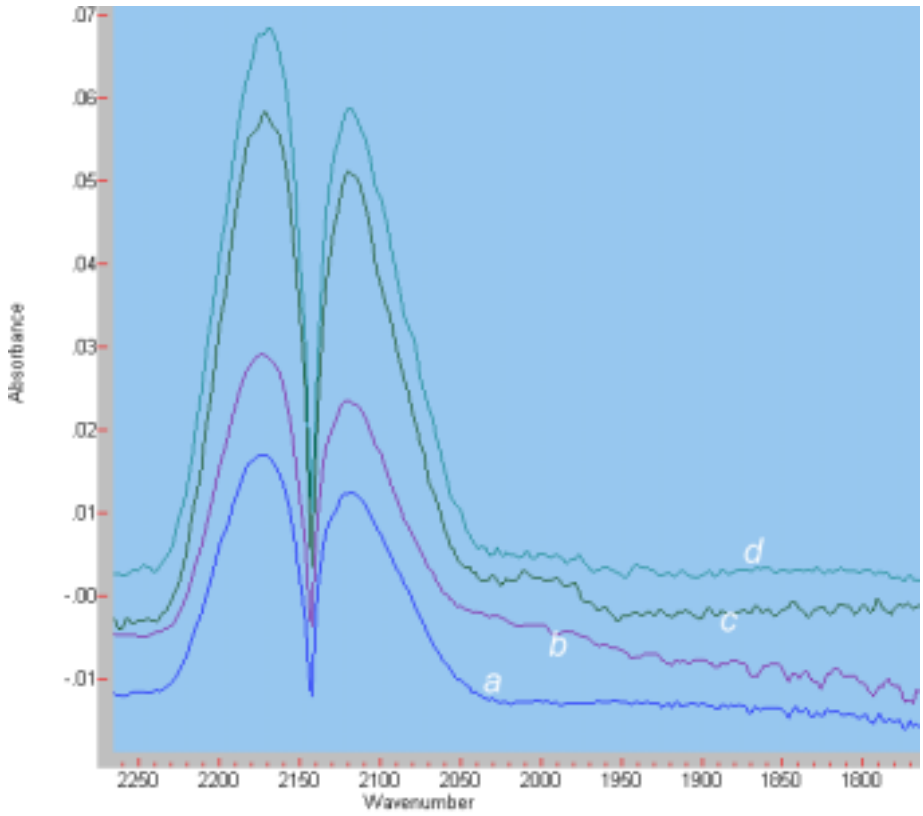

Fig. 3.27: DRIFTS spectra of CO region for gold containing samples; a) Cat1, b) Cat2, c) Cat4, d) Cat3

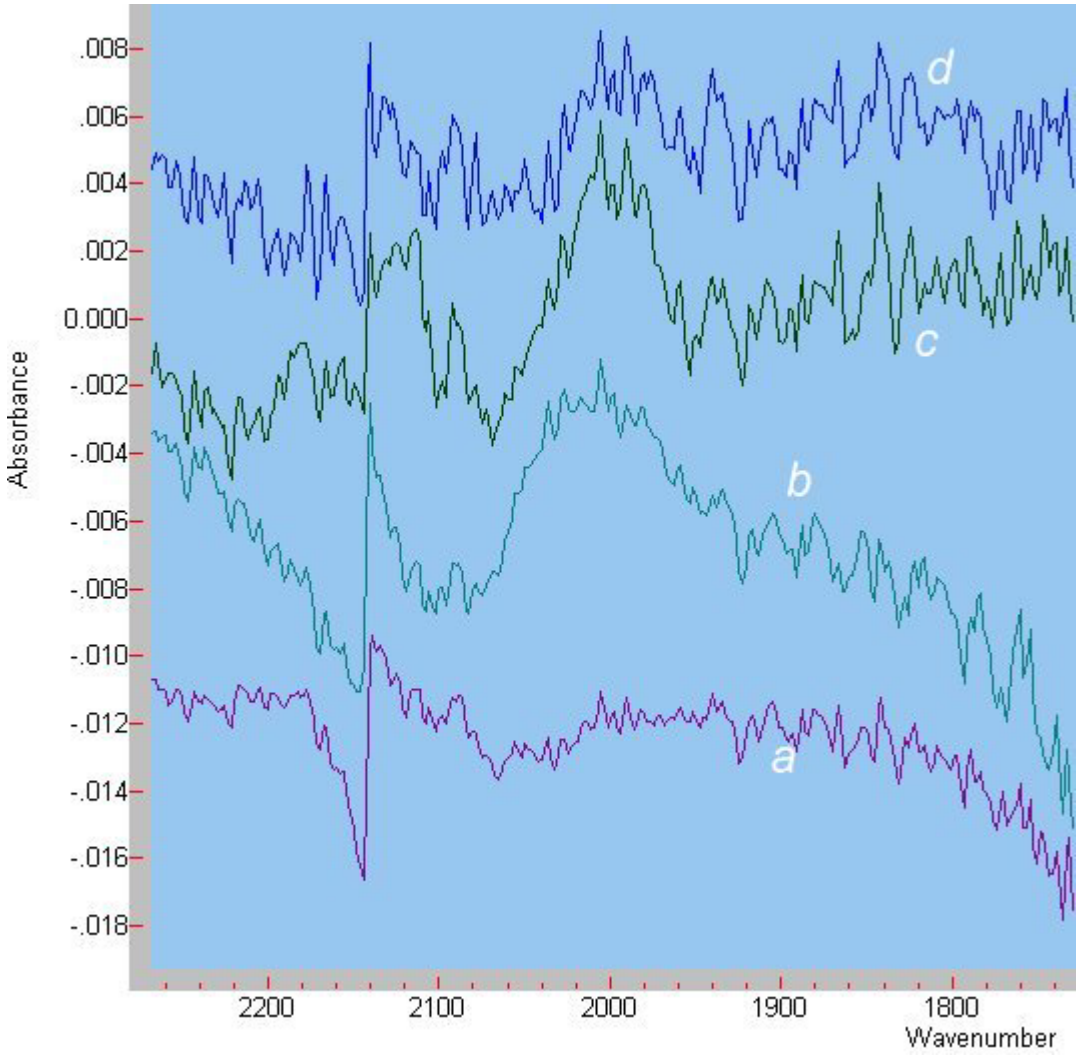

Fig. 3.28: DRIFTS spectra of gold containing samples after subtraction of gas phase CO peaks; a) Cat1, b) Cat2, c) Cat4, d) Cat3

The most obvious feature is present at 2143 cm^{-1} due to miscancellation of the gas phase spectra from Fig. 3.27. Thereafter a weak feature is obvious at 2005 cm^{-1} for Cat2, Cat3 and Cat4, but absent in Cat1. Much weaker features, close to the noise level are also present at 1932cm^{-1} for Cat2, Cat3 and Cat4 and 2086cm^{-1} for all spectra.

3.6 Mass Spectroscopy

The absolute sensitivity of the instrument and the sampling efficiency varied between experiments, so the CO_2 production levels were normalised for easy comparison. The signal at mass 28 for inlet CO through the bypass prior to experiment was used to normalise the CO_2 results to give a relative yield. As can be seen from the graph, this procedure resulted in large errors as the three samples that appear to have reached 100% conversion (Blank1, Cat2, Cat4) have reached a plateau at different values. The normalised production of CO_2 with temperature is illustrated in Fig. 3.29.

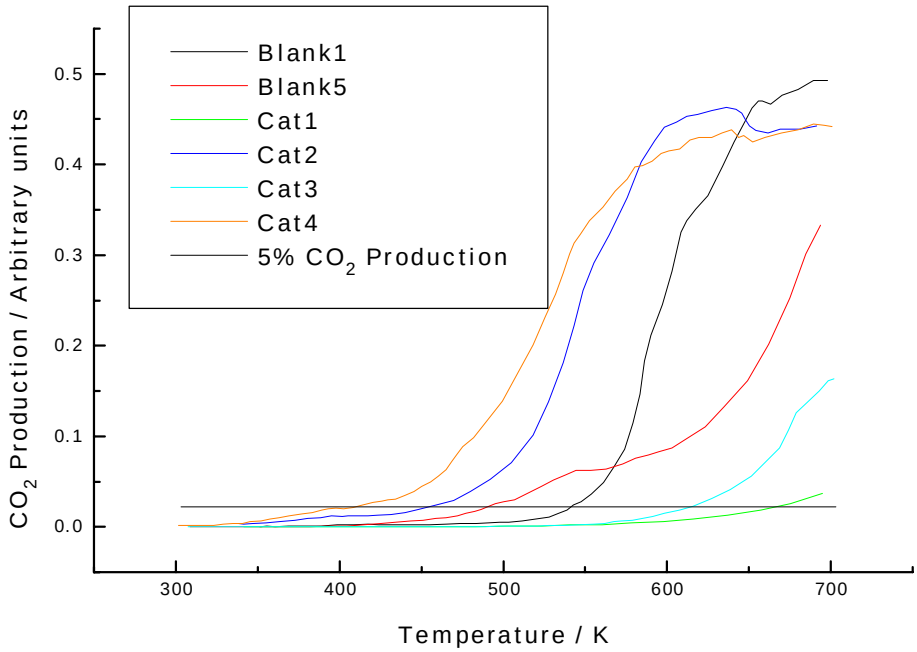

Fig. 3.29: Graph of normalised CO_2 production for all samples, with line of 5% production

As the catalysts varied widely in activity, the temperature for 5% conversion ($T_{5\%}$), measured by production of CO_2 was taken as a measure of relative activity. These values are given in Table 3.5.

Sample	Synthesis	5% Conversion Temperature /K
Blank1	As-precipitated 1	543
Blank5	Combustion	491
Cat1	As-precipitated 1	667
Cat2	As-precipitated 1	455
Cat3	Combustion	614
Cat4	As-precipitated 2	410

Table 3.5: Activity of all samples reported as temperature at which 5% production of CO_2 is reached

Chapter 4: Discussion

4.1 Mass spectroscopy

The mass spectroscopy results are vitally important as they represent the activity of the catalysts for the desired reaction. The activity for the low temperature oxidation of CO is the most interesting and important section of the study as it is the relationship between this property and the morphology of the catalysts that can provide an understanding of the mechanism.

A common method of reporting the activity of catalysts is the temperature of 50% conversion, or $T_{1/2}$. This value is most often quoted for a flow of 1% CO balanced to 67sccm min $^{-1}$ with air over approximately 200mg catalyst. This equates to a flow of 3.35 $sccm_{CO}$ g_{cat}^{-1} min^{-1}. Harutas co-precipitated catalyst manages a $T_{1/2}$ of 346K [32], with the as-precipitated catalysts of Iwasawa *et al.* managing a $T_{1/2}$ of 206K [21]. Another method reported, which is closer to that used here has 3.3% CO and 1.6% O_2 balanced to a flow of 150 sccm min^{-1} over 150mg catalyst [56]. This is a flow of 30 $sccm_{CO}$ g_{cat}^{-1} min^{-1}. In this case the temperature for 4% conversion ($T_{4\%}$) is reported, with the best value being 242K. The regime for this project gives a flow of approximately 20 $sccm_{CO}$ g_{cat}^{-1} min^{-1} and 10 $sccm_{O2}$ g_{cat}^{-1} min^{-1}.

The activities of the catalysts prepared in this study are given in Table 4.1. The most active catalyst was Cat4, followed by Cat2. These catalysts were generally similar in activity and considerably more active than the next most active material, which was in fact Blank1, followed by Blank5 and Cat3, with the lowest activity form Cat1. Overall the range of activity noted was wide, with the temperature for 5% conversion varying between 410 and 667K. In comparison with the activities of the literature materials the best catalyst synthesised here could only manage $T_{1/2}$ of 524K, and the best $T_{5\%}$ was a disappointing 410K.

Sample	Synthesis	5% Conversion Temperature /K
Blank1	As-precipitated 1	543
Blank5	Combustion	491
Cat1	As-precipitated 1	667
Cat2	As-precipitated 1	455
Cat3	Combustion	614
Cat4	As-precipitated 2	410

Table 4.1: Activity of all samples reported as temperature at which 5% production of CO_2 is reached

Another method for measurement of activity is the turnover frequency (TOF). This is a measure of how many molecules on average are reacted (turned over) on an active site of a catalyst in a second. As there is no reliable method for determining the surface area of gold, any TOF for these systems is an estimate based on a calculated approximation of the surface area. Iwasawa has reported a calculated TOF of 17.9×10^3 s^{-1} for an as-precipitated Au/Fe_2O_3 catalyst at 207K [57]. The number of active gold sites was estimated from the mean diameter of gold particles assuming a hemispherical shape. The 5% CO_2 production quoted for the samples produced here is equivalent to a conversion of 1.773×10^{17} molecules g_{cat}^{-1} s^{-1}. For a rough comparison, assuming 3% loading of gold and that between 100% and 0.01% of the gold atoms are active sites, this gives a TOF of between 1.933×10^{-3} s^{-1} and 19.33 s^{-1} for 5% conversion at the various temperatures.

All of the values of activity, regardless of the method of expression, given in the literature for gold catalysts are substantially higher than those reported in this study. With respect to other catalytic systems, a study on Pt catalysts [58], reports activities that are closer to those obtained in this study. A TOF was reported as 3.6×10^{-3} s^{-1} at 423K for a Pt/Al_2O_3 catalyst with a $T_{1/2}$ of 453K. This shows that the best catalysts in this study are at least comparable with other systems.

Although the principal reaction of the catalysts under the CO/O_2/He feed used here was CO oxidation, all of the catalysts showed some production of methane as a side product, and Cat4, Blank5 and Blank1 also displayed hydrogen production. The order of reactivity for methane production was the same as that for the CO oxidation, with Cat4 the most active. For the production of hydrogen, Blank5 was the most active, followed by Blank1 and Cat4. The gases produced by Blank5 are shown in Fig. 4.1. Note the break in slope for the production of CO_2 when H_2 production starts.

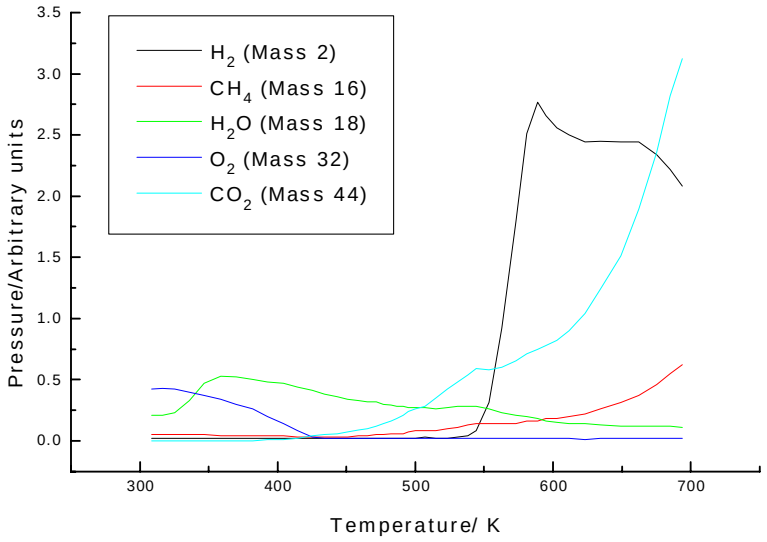

Fig. 4.1: Gases evolved over Blank5 on heating under reaction flow

It is likely that the reverse water gas shift reaction (1) is occurring, to produce hydrogen that reduces the carbon monoxide in a CO methanation reaction (2):

1 $CO + H_2O \rightarrow CO_2 + H_2$

2 $CO + 3\ H_2 \rightarrow CH_4 + H_2O$

The two reactions shown above depend on each other as well as the primary reaction of oxidising CO to CO_2, and the availability of sufficient H_2O in the gas feed stream. Each reaction will be sensitive to each other and the relative rates at

different times will depend on the partial pressures of CO, CO_2, H_2, H_2O and CH_4, as well as the temperature and total pressure. This interdependence makes the interpretation rather difficult, and no further attempt was made.

In the literature, no mention is made of the side reactions on Au catalysts in general producing hydrogen and methane, but these reactions may be a function of the activity of the iron oxide support, rather than the supported gold itself. This is supported by the fact that the blank samples are more reactive than two of the catalysts, with the greatest production of hydrogen occurring on Blank5. Iron oxide catalysts have been commonly used for the water gas shift reaction, and methanation is essentially the simplest form of Fischer-Tropsch catalysis for which iron oxide based materials are commonly used [59]. If it is the case that the reaction is purely progressing on the support, the highly active gold catalysts reported would not show any side reactions as the temperature for the support to react in this way is much higher than that normally seen for the oxidation of carbon monoxide over the gold.

4.2 Surface Area

The BET surface areas of the various catalysts are given in Table 4.2, along with literature values for comparison. Values range from 37 to 134 m^2g^{-1}, with those of Cat2 and Cat4 substantially higher than those reported in the literature. However, the other samples have values closer to those previously reported. In general, iron oxides tend to have low surface areas, although high area forms can be synthesised. No literature values could be found for combustion synthesised iron oxide. As reported earlier, production of the catalysts is highly sensitive towards the synthesis, and the range of surface areas, along with the varying activity seem to bear this out.

Sample	Synthesis	BET Surface area (m^2g^{-1})	Reference
Blank1	As-precipitated 1	54	This work
Blank5	Combustion	39	This work
Cat1	As-precipitated 1	37	This work
Cat2	As-precipitated 1	119	This work
Cat3	Combustion	48	This work
Cat4	As-precipitated 2	134	This work
Au/Fe_2O_3	As-precipitated 2	54	57
Au/Fe_2O_3	As-precipitated 2	63	21
Au/Fe_2O_3	Co-precipitation	73	32
Au/Fe_2O_3	Co-precipitation	37	35

Table 4.2: Surface area of samples and literature values by BET measurement

4.3 XRD

The powder XRD shows that two support phases are dominant in all of the crystalline samples. Within these materials the dominant phases are haematite, and magnetite or maghemite (γ-Fe_2O_3) (the XRD patterns of the two materials are identical due to the fact that maghemite is isostructural with magnetite, but contains cation deficient sites). Of the crystalline catalysts, Cat 3 appears to have the greatest proportion of magnetite or maghemite, followed by Cat2, with Cat1 being mainly haematite. It has hard to state this categorically, due to some of the peaks overlapping and the dependence of the peak form on support crystal morphology. Also present on Cat1 are some peaks at 14.7°, 20.6° and 27.5°. The phase responsible for these peaks was not identified. Cat4 shows the lowest crystallinity with no obvious diffraction features due to any phase of iron oxide.

The above findings are similar to those reported in the literature. Iwasawa reports phases of hematite and maghemite only in a preparation of as-precipitated catalysts similar to that reported here [57], while Haruta claims that the iron oxide formed by coprecipitation is predominantly hematite [6].

Using the Scherrer equation to estimate the gold particle size gives varied results, which are displayed in Table 4.3 with the experimental results. The range of size is surprisingly large for materials with similar syntheses, with values between 42 and 139 nm. The gold particles obtained were substantially larger than those reported in the literature. As precipitated catalysts have shown no gold peaks, showing that the particle size is less than 4nm [21]. The catalysts prepared by coprecipitation and impregnation are reported as having larger particles than those using the as-precipitated technique. However, these are still appreciably smaller than those synthesised here.

Sample	Synthesis	Average size/nm	Ref
Cat1	As-precipitated 1	71	This work
Cat2	As-precipitated 1	139	This work
Cat3	Combustion	74	This work
Cat4	As-precipitated 2	42	This work
Au/Fe_2O_3	Co-precipitation	3.6	32
Au/Fe_2O_3	Impregnation	16	32
Au/Fe_2O_3	As-precipitated 2	<4	21

Table 4.3: Size of gold particles as calculated using Scherrer equation, including literature values for comparison

4.4 TEM

The range of gold particle sizes given by TEM is fairly narrow, being between 18.7 and 29.7 nm. These values are again large compared with those in the literature; for example, Iwasawa quotes values for an as-precipitated Au/Fe_2O_3

catalyst as 4.1nm [57], whilst a coprecipitated catalyst was reported with an average particle size of 2.6nm by Haruta [32]. The size of gold particles as estimated by TEM disagreed with that estimated from the XRD results, with the TEM consistently underestimating the size. With TEM good contrast between the gold and iron oxide support is only available when the electrons can easily penetrate the support, which happens when the support is thin, generally at the edges of support fragments.
Particle sizes and size statistics are only available form a small section of the bulk of the catalyst and therefore not necessarily totally representative. Although this potentially explains the difference in results when using these two methods, it is still worth noting that XRD suggests that Cat4 has the smallest particles, followed by Cat1, Cat3 and Cat2, whereas the TEM has the order as Cat2, Cat4 and Cat1, with there being no obvious gold particles on Cat3 whatsoever.

4.5 SEM

The secondary electron detector micrographs show a morphology that seems not to vary substantially between the samples and no variation in the crystallinity of the samples is noticeable. The SEM images should provide a crude idea of the surface area for the samples, as the finer the grain appearing in the sample, the more surface will be present. However, the SEM images are not significantly different in this regard, and as the difference between the lowest and highest surface areas is only a factor of four, this would not be expected to be immediately obvious to the eye.

The back scattering detector images show the varied morphology of the gold species in a complementary manner to the TEM. Cat4 shows very few particles at low magnification, whilst at high magnification particles are appearing at the limits of resolution. The other catalysts show gold particles at lower magnification, with Cat2 and Cat3 also showing some much larger particles of amorphous form. This suggests sintering of the gold into larger forms, although another explanation for this could be poor mixing of the gold precursor with the support, in the case of Cat2, or support precursor for Cat3, but this seems unlikely.

EDS analysis of the materials associated with the SEM imaging confirmed the presence of Au in the catalyst materials and also indicated amounts of other elements at lower levels presumably associated with contamination or impurities in the reagents used in the syntheses. Unfortunately EDS is only a semi-quantitative method and does not allow detailed comparison of the amounts of elements found. The technique is also spatially dependent, as it relies in the size and position of the electron beam on the sample.

This effect is shown below in Fig. 4.2, where the two spectra are from different points on the same sample. The huge difference in relative intensities of the peaks due to iron and gold illustrate the disadvantages of this technique.

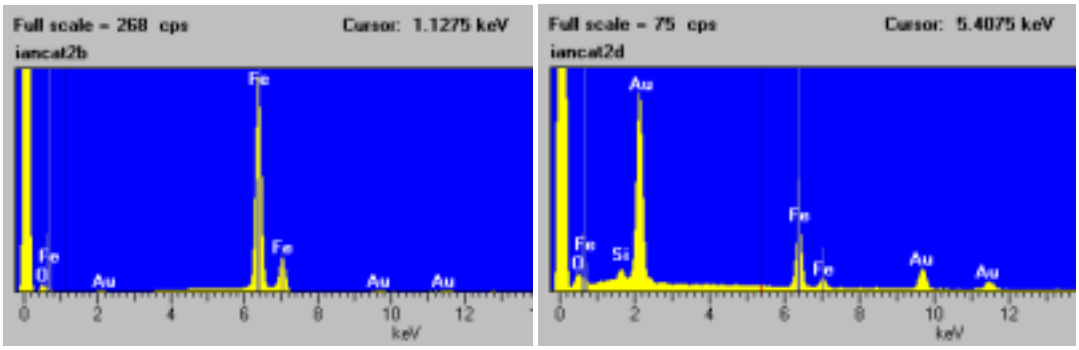

Fig. 4.2: Two EDS spectra from different points showing spatial variability of the technique

EDS analysis of the blank pads used to mount the powdered catalysts samples for SEM/EDS showed only sulfur and carbon, sodium and oxygen. The sulfur and carbon do not feature in the EDS spectra of the catalyst samples, showing that when the sample is covering the pad it prevents the detection of elements. It is therefore safe to assume that the sodium detected in Blank1 is present in the sample. The EDS also indicated that the two most reactive samples, Cat2 and Cat4, contain traces of silicon. Another point worth noting is the presence of two elements commonly referred to as poisons and promoters in the literature. Chlorine is present in Cat3, and may be the reason for its low activity, although the method of synthesis may not provide the necessary interaction between the gold and support.

4.6 XPS

The interpretation of XPS spectra can be undertaken on two levels. The intensity of a peak shows the amount of a species present on the surface of a sample, whilst the peak position provides information on the oxidation state of the species. As the process of obtaining XPS spectra can be rather time consuming, it is common to take a survey scan of the entire spectral range at low resolution before focussing on regions of interest with greater precision.

XPS results for active Au/Fe_2O_3 catalysts are presented in a number of studies in the literature. Data is available not only for the Fe, Au and O regions, but also the phosphorus 2p region, where calcined materials have shown a P peak shifted to high binding energy compared to the uncalcined as prepared catalysts [19,20]. This is explained by the oxidation of the triphenlyphosphine ligand to a P^{5+} species in the calcination step. The binding energy is reported as 133.3eV on Fe_2O_3 support. The weak P features noted here in the XPS spectra of Cat1 and Cat2, although at a slightly higher binding energies are still thought to arise in a similar manner.

There are few reports of the Fe 2p region in the literature, but a study of coprecipitated and impregnated catalysts by Galvagno *et al.* gives the spectra [41]. They suggest that there is little variation between the catalysts they prepare, with the main peak at 711.4 eV, and satellite peaks characteristic of Fe^{III} between 715 and 720 eV. When the samples are reduced under a stream of hydrogen the peaks shift to lower binding energy and the satellite peaks weaken. The spectra from the iron 2p region for the catalysts in this study show that the iron is in a very similar state for all of the samples, except Cat1 and Blank1, and these values are close to those reported in the literature, although again a little high. The shift of the peaks on Cat1 and Blank1 to lower binding energy, like the reduced sample in the study above, suggests a lower oxidation state, although due to the large number of phases of iron oxides, it is difficult to assign the exact phase to each of the samples.

The study of the gold on supported gold catalysts by XPS has concentrated on the Au 4f region. Haruta found that an active catalyst prepared by coprecipitation had an Au $4f_{7/2}$ peak at 84.0 eV which was assigned to metallic gold [35]. Galvagno found that a peak at 86.5 eV, which was assigned to Au^{III} shifted to 83.8 eV with time on stream, i.e. the gold was reduced to the metal. The Au $4f_{7/2}$ results obtained in this study showed the peaks due to Cat2 and Cat4 were at 85 eV, whereas Cat1 had a peak at 84 eV. The Au $4f_{5/2}$ peak shows a larger shift from 87 to 89 eV. These factors suggest that the gold on Cat2 and Cat4 is present as Au^{+}.

An estimate of the Au loading of the catalysts based simply on the relative intensity of the Au feature in XPS results does not agree with the other gold loadings calculated from the synthesis, as Cat4, which has the highest calculated loading has a response much lower than that of Cat1 or Cat2. Also no gold was detected on Cat3, which is contrary to the results from the EDS and the SEM. Due to the fact that the XPS has a limited sampling depth, it is possible that the gold is present, but not on the surface, allowing it to be imaged/detected by the high energy electrons used in the microscopy experiments but not the comparatively low energy photoelectrons generated in the XPS experiment. Cat3 does have the lowest gold loading, so it may simply be that the XPS is not sensitive enough to detect the gold, although it is unlikely that the instrument could detect impurities in the other samples more successfully than one of the elements designed to be incorporated in Cat3.

4.7 IR

In the literature, IR spectroscopy has been applied to virtually all of the studied gold catalysts in varying forms [20,21,60]. Only a few DRIFTS studies have been undertaken [7,15,37], with fewer of these concerned with iron oxide support [7], and no DRIFTS studies were found using as-precipitated gold/iron oxide catalysts. A number of these studies were also hoping to discover the mechanism and used isotopic probes of molecules containing ^{13}C and ^{18}O [45,61].

Of the peaks detected in the DRIFTS experiments described here, the only reliable one is the broad peak centred around 2005cm^{-1}. This is strongest on Cat4, followed by Cat2, then Cat3 and finally Cat1. The other potential peaks noted at 1932 and 2086 cm^{-1} are at the limits of detection, and could easily be due to some miscancellation, or artefact introduced by subtraction of the gas phase spectrum. For the assignation of peaks, the lowest wavenumber peak due to adsorbed CO on Au found in the literature was 2040cm^{-1} on an impregnated MgO supported catalyst [60]. Bollinger and Vannice report a broad peak at 2038 cm^{-1} for a TiO_2 supported gold catalyst [14]. This peak however, was not assigned, although in the same study a gold adsorbed CO peak was found at 2105 cm^{-1}. The closest match found to the peak

at 2086cm^{-1} is adsorbed CO on an impregnated Au/MgO catalyst at 2085cm^{-1} [62]. There are no reports of any peaks due to CO adsorbed on the metal below 2030cm^{-1}. As the catalysts produced here have a much lower activity than previously reported, a difference must be present between them. It therefore follows that the spectrum of adsorbed CO would be different. However, it should be noted that the relative activity of the catalysts increases with the magnitude of this peak.

4.8 Conclusions

Overall, the results of the study must be considered somewhat disappointing as the activity of the catalysts prepared, although not dissimilar to other Pt based oxidation catalysts, do not rival those reported in the literature for other Au based systems. The collected results from the characterisation of the materials do however point towards some common features of the more active samples.

The gold particle sizes given by different methods showed a variation that is rather unwelcome. The TEM consistently gave lower values than the Scherrer analysis, and the SEM showed the presence of some irregular particles of much greater size for some of the catalysts. Here, the Scherrer analysis of the XRD data is considered to give the best estimate of size, as the data analysed is more representative of the entire sample volume than for TEM or SEM.

The size of the gold particles has been shown to have little effect on the activity of catalysts when supported on active supports such as iron oxide, but a great effect when on inert supports [27]. This is due to the interaction between the gold and the support. A size effect will therefore be present as on an inert support if the gold is not properly and intimately attached to the iron oxide. Cat4 has the smallest gold particles and the highest activity, but Cat2 has the largest particles, but still retains a high activity. This shows that size is not the only important factor for high activity in this study.

The nature of the support is shown to vary from one synthesis to another by the measurements of the surface area, the XRD patterns, the TEM and the XPS

spectra. It would be expected that catalysts with high surface areas would give the highest activity.

The highest surface areas do indeed belong to the catalysts with the highest activity in this study, although the variation of activity between the less active catalysts cannot be explained in this way. The difference between the surface area values in the literature and those reported here also shows that this is not the sole reason for the high activity of Au/Fe_2O_3 catalysts.

The XRD shows Cat4 as the most amorphous catalyst and this agrees with the hypothesis that amorphous supports are more active [21]. Cat1 is however less crystalline than Cat1 or Cat3, yet has the lowest activity of all the samples. Cat2 is only slightly less active than Cat4, but has much sharper XRD peaks. The inactivity of Cat1 could be explained by reference to the unknown peaks, suggesting that the catalyst is poisoned by some contaminant. This would also explain why Cat1 is less reactive than the blank samples, which contain no gold. The absence of detectable gold on Cat3 in both the TEM and XPS may be explained by the synthesis. Whereas the as-precipitated method relies on supporting the gold on a previously synthesised material, the solution combustion method is more likely to result in the incorporation of gold into the bulk. This would obviously also result in a much lowered reactivity.

The nature of the interaction between gold and support needed for the high activity is still under debate, but it is likely that it is either completely absent, or present only weakly in the materials synthesised here. This is backed up by the spherical particles found in the TEM, the large gold particles formed by sintering, and the activity of the catalysts. The importance of careful attention to the synthesis is widely reported within the literature, and this study clearly reinforces this point.

Although it has not been possible to determine the factors necessary to produce highly active gold catalysts, a number of features have been identified that are common to the more active samples. The strength of the adsorbed CO peak at 2005 cm^{-1} correlates with the activity of the catalysts. This is presumably due to the presence of a form of CO that has the energy barrier for reaction lowered. The

identification of the genesis of the energy shift in the CO molecule could provide a useful insight into the mechanism present in gold catalysed CO oxidation.

The XPS shows that the most active catalysts have gold present in the cationic form, whilst the poorest has metallic gold. This result could explain the IR results and provides a plausible active site for the reaction to occur upon. Further, this relatively small difference between the more and less active materials is consistent with the highly sensitive nature of the synthesis.

Finally, the two catalysts (Cat2 and Cat4) that are much more active than the others have a higher surface area. This basic feature is one that is very important in catalytic activity and hints towards a better synthesis technique in their production. A high surface area is rarely detrimental in catalysis, and those reported here are very competitive with those in the literature.

Further work upon this project would be useful in the measurement of activity with dried gases, so that the reverse water gas shift reaction could be eliminated and the results much simplified. Further study could also focus upon the nature of the interaction between the gold and support by comparison with a highly active catalyst, or concentrate upon the production of such a catalyst, maybe refining the combustion synthesis. However, as the production of as-precipitated catalysts does depend so crucially upon the synthesis, which has been reported successfully only seldomly, it is unlikely to be commercially viable in light of the alternative routes to supported gold catalysts which are cheaper and more reliable.

Bibliography

1. B.Trapnell, *Proc.Roy.Soc., Sr.A* **218**, 566, 1953.

2. N.Endow, B.Wood, and H.Wise, *J.Catal.* **15**, 136, 2001.

3. N.W.Cant and P.W.Fredrickson, *J.Catal* **37**, 531, 1974.

4. N.W.Cant and W.K.Hall, *J.Phys.Chem.* **75**, 2914, 1971.

5. H.Huber, D.McIntosh, and G.A.Ozin, *Inorg.Chem.* **16**, 975, 1977.

6. M.Haruta, T.Kobayashi, H.Sano, and N.Yamada, *Chem.Lett.* 405, 1987.

7. M.M.Schubert, M.J.Kahlich, H.A.Gasteiger, and R.J.Behm, *J.Power Sources* **84**, 175, 1999.

8. M.J.Bollinger, R.E.Sievers, D.W.Fahey, and F.C.Fehsenfeld, *Anal.Chem.* **55**, 1980, 1983.

9. W.S.Epling, G.B.Hoflund, J.F.Weaver, S.Tsubota, and M.Haruta, *J.Phys.Chem.* 9929, 1996.

10. Personal communication from Matsushita Housing Products Co. to M. Haruta [71]

11. A.Ueda and M.Haruta, *Shigen Kankyo Taisuaku (Resources and Environment)* **28**, 1035, 1992.

12. Y.Iizuka, T.Tode, T.Takao, K.Yatsu, T.Takeuchi, S.Tsubota, and M.Haruta, *J.Catal* **187**, 50, 1999.

13. Y.J.Chen and C.T.Yeh, *J.Catal* **200**, 59, 2001.

14. T.Kobayashi, M.Haruta, S.Tsubota, and H.Sano, *Sens and Actuators* **131**, 222, 1990.

15. M.Bollinger and M.Vannice, *Appl.Cat.B* **8**, 417, 1996.

16. Y.Yuan, K.Asakura, H.Wan, K.Tsai, and Y.Iwasawa, *Chem.Lett.* **755**, 1996.

17. A.M.Mueting, B.D.Alexander, P.D.Boyle, A.L.Casalnuovo, L.N.Ito, B.J.Johnson, and L.H.Pignolet, *Inorganic Syntheses* **29**, 280, 1992.

18. F.Cariati and L.Naldini, *J.C.S.Dalton* 2286, 1972.

19. A.I.Kozlov, A.P.Kozlova, H.C.Liu, and Y.Iwasawa, *Appl.Cat.A* **182**, 9, 1999.

20. A.P.Kozlova, A.I.Kozlov, S.Sugiyama, Y.Matsui, K.Asakura, and Y.Iwasawa, *J.Catal* **181**, 37, 1999.

21. A.P.Kozlova, S.Sugiyama, A.I.Kozlov, K.Asakura, and Y.Iwasawa, *J.Catal* **176**, 426, 1998.

22. J.Steggerda, J.Bour, and J van der Velden, *J.R.Net.Chem.Soc.* **101**, 164, 1982.

23. M.Haruta, *Catal.Today* **36**, 153, 1997.

24. C.Sze, E.Gulari, and B.Demczyk, *Mater.Res.Soc.Proc.* **286**, 143, 1993.

25. S.D.Lin, M.Bollinger, and M.A.Vannice, *Catal.Lett.* **17**, 245, 1993.

26. G.K.Bethke and H.H.Kung, *Appl.Cat.A* **194-195**, 43, 2000.

27. R.Finch, N.Hodge, G.J.Hutchings, A.Meagher, Q.Pankhurst, M.R.H.Siddiqui, F.E.Wagner, and R.Whyman, *Phys.Chem.Chem.Phys* **1**, 485, 1998.

28. M.M.Schubert, S.Hackenberg, A.C.van Veen, M.Muhler, V.Plzak, and R.J.Behm, *J.Catal* **197**, 113, 2001.

29. I.W.Bassi, F.W.Lytle, and G.Parravano, *J.Catal* **42**, 139, 1976.

30. Y.Yuan, A.P.Kozlova, K.Asakura, H.Wan, K.Tsai, and Y.Iwasawa, *J.Catal* **170**, 191, 1997.

31. Y.Kang and B.Wan, *Catal.Today* **26**, 59, 1995.

32. M.Haruta, N.Yamada, T.Kobayashi, and S.Iijima, *J.Catal* **115**, 301, 1989.

33. R.M.Cornell and U.Schwertmann, In "The Iron Oxides" VCH, Weinheim, 1996.

34. P.Bera, K.Patil, V.Jayaram, G.Subbanna, and M.Hegde, *J.Catal* **196**, 293, 2000.

35. P.Bera, K.Patil, V.Jayaram, M.Hegde, and G.Subbanna, *J.Mat.Chem.* **9**, 1801, 1999.

36. P.Bera, S.Aruna, K.Patil, and M.Hegde, *J.Catal* **186**, 36, 1999.

37. A.K.Tripathi, V.S.Kamble, and M.N.Gupta, *J.Catal* **187**, 332, 1999.

38. M.Haruta, S.Tsubota, T.Kobayashi, H.Kageyama, M.J.Genet, and B.Delmon, *J.Catal* **144**, 175, 1993.

39. J.D.Grunwaldt, M.Maciejewski, O.S.Becker, P.Fabrizioli, and A.Baiker, *J.Catal* **186**, 458, 1999.

40. E.Park and J.Lee, *J.Catal* **186**, 1, 1999.

41. A.M.Visco, F.Neri, G.Neri, A.Donato, C.Milone, and S.Galvagno, *Phys.Chem.Chem.Phys* **1**, 2869, 1999.

42. J.Frost, *Nature* **334**, 577, 1988.

43. Y.Iizuka, H.Fujiki, and M.Haruta, Unpublished work [7]

44. M.Valden, X.Lai, and D.W.Goodman, *Science* **281**, 1647, 1998.

45. F.Boccuzzi, A.Chiorino, S.Tsubota, and M.Haruta, *Catal.Lett.* **29**, 255, 1994.

46. H.Liu, A.I.Kozlov, A.P.Kozlova, T.Shido, K.Asakura, and Y.Iwasawa, *J.Catal* **185**, 252, 1999.

47. M.Olea, M.Kunitake, T.Shido, and Y.Iwasawa, *Phys.Chem.Chem.Phys* **3**, 627, 2001.

48. H.Liu, A.I.Kozlov, A.P.Kozlova, T.Shido, and Y.Iwasawa, *Phys.Chem.Chem.Phys* **1**, 2851, 1999.

49. Personal communication from Y.Iwasawa, to G.McDougall 2001.

50. K.Patil, S.Aruna, and S.Ekambaram, *Current opinion in solid state and materials science* **2**, 158, 1997.

51. P.Bera, K.Patil, and M.Hegde, *Phys.Chem.Chem.Phys* **2**, 373, 2000.

52. "Powder Diffraction File Inorganic Phases Search Manual." JCPDS International Centre for Diffraction Data, Pennsylvania 1982.

53. M.Cavers, PhD thesis, University of Edinburgh 2000.

54. P.F.Barron, L.M.Engelhardt, P.C.Healy, J.Oddy, and A.H.White, *Aust.J.Chem.* **40**, 1545, 1987.

55. S.Galvagno and G.Parravano, *J.Catal* **55**, 178, 1978.

56. F.E.Wagner, S.Galvagno, C.Milone, A.M.Visco, L.Stievano, and S.Calogero, *J.Chem.Soc.Faraday Trans* **93**, 3403, 1997.

57. A.I.Kozlov, A.P.Kozlova, K.Asakura, Y.Matsui, T.Kogure, T.Shido and Y.Iwasawa, *J.*Catal **196,** 56, 2000.

58. Y.J.Mergler, A.van Aalst, J.van Delft and B.E.Nieuwenhuys, *Appl.Cat.B* **10**, 245, 1996.

59. B.H.Davis, D.R.Milburn, K.V.R.Chary and R.J.O'Brien, *Appl.Cat.A* **180**, 277, 1999.

60. J.Y.Lee and J.Schwank, *J.Catal* **102**, 207, 1986.

61. F.Boccuzzi, A.Chiorino, S.Tsubota and M.Haruta, *J.Phys.Chem* **100**, 3625, 1996.

62. J.Schwank, G.Parravano, and H.L.Gruber, *J.Catal* **61**, 19, 1980.